



Mechanistic insights and consequences of intrapore liquids in ethene, propene, and butene dimerization on isolated Ni²⁺ sites grafted within aluminosilicate mesopores



Iker Agirrezabal-Telleria, Enrique Iglesia*

Department of Chemical and Biomolecular Engineering, University of California at Berkeley, Berkeley, CA 94720, USA

ARTICLE INFO

Article history:

Received 27 April 2020

Revised 23 June 2020

Accepted 28 June 2020

Available online 6 July 2020

Keywords:

Alkene dimerization
Intrapore condensation
Stabilization
Subambient temperature
Ni-Al-MCM-41 catalysts
Reaction mechanism

ABSTRACT

The stability, selectivity, and reactivity conferred by intrapore liquids onto Ni²⁺ species grafted within mesoporous aluminosilicates for the dimerization of C₂–C₄ alkenes are reported and interpreted by the preferential stabilization of dimer desorption transition states, which inhibit further growth during the surface sojourn that forms these dimers. The marked decrease in deactivation rate constants leads to catalyst half-lives > 600 h for all alkenes and to turnover rates (per Ni) at sub-ambient temperatures (240–260 K) that exceed those at the higher temperatures previously used for Ni-based solid catalysts (350–500 K). These effects appear at the relative pressures required for alkene capillary condensation within Ni-Al-MCM-41 catalysts with different mesopore diameters and are also evident when the intrapore liquids consist of unreactive alkanes, indicative of solvation effects conferred by non-covalent interactions mediated by dispersion forces. For all alkenes, turnover rates (per Ni) are unaffected by Ni content until each acidic proton in the Al-MCM-41 is replaced by one Ni atom, consistent with the involvement of grafted (Ni-OH)⁺ monomers as active centers and excess Ni leading to inactive NiO species. The stable nature of these catalysts allows accurate mechanistic assessments and a demonstration of the kinetic relevance of the C–C coupling elementary steps on essentially bare (Ni-OH)⁺ centers, leading to rates described by second-order dimerization constants (α'_n) and adsorption constants (β'_n) for each alkene (C_n); these parameters are influenced only slightly by intrapore liquids, because they reflect free energies of formation of surface-bound species and transition states from gaseous precursors. These α'_n and β'_n parameters increase with alkene size, with the enthalpic component of α'_n increasing from 21 to 46 kJ mol⁻¹ and the activation entropy becoming more negative (–103 to –187 J (mol K)⁻¹), consistent with C–C coupling transition states that occur late along the reaction coordinate and resemble its bound dimer product. The low C_{3n}/C_{2n} ratios observed in the presence of intrapore liquids (<0.04, for n = 2–4) reflect the endothermic nature of dimer desorption events, for which product-like transition states benefit from the solvation of desorbing products by a non-polar liquid phase, thus allowing detachment from Ni centers before subsequent growth. The inhibition of such growth events accounts not only for the unique dimer selectivity observed, but also for the unprecedented stability conferred by intrapore liquids by inhibiting the formation of oligomers that bind more strongly with increasing chain size, as evident from the β'_n values reported here for alkene reactants.

© 2020 Elsevier Inc. All rights reserved.

1. Introduction

The formation of new C–C bonds from alkenes through dimerization routes provides practical paths for the growth of hydrocarbon chains in the production of fuels and chemicals [1,2]. These reactions proceed at moderate temperatures (ca. 400 K) on solid Brønsted acids, such as zeotypes that contain protons within voids

of molecular dimensions [3–7]. They are also catalyzed by cationic Ti, Cr, and Ni centers as solvated organometallic complexes [8–13] or grafted onto porous solids [14,15]. Organometallic complexes [16,17] and Ni-based organic frameworks (MOF) [18–21] function at near-ambient temperatures with higher dimerization rates (per Ni atom) and primary ethene dimer selectivities than Brønsted acids [7,8]. They require, however, aluminoxane moieties in large excess as activators or co-catalysts, as well as liquid solvents as the reaction media. Ni cations grafted onto mesoporous aluminosilicates, such as Al-SBA-15 [22] and Al-MCM-41 [23–29], can

* Corresponding author.

E-mail address: iglesia@berkeley.edu (E. Iglesia).

function without activators or solvents; they often give rise to ethene dimerization rates similar to those on organometallic complexes, but at higher temperatures and with lower selectivity to primary 1-butene dimers.

Ni-based solids also deactivate rapidly [19,22], especially for larger alkenes, because larger oligomeric species form occasionally and bind more strongly onto active centers than the parent constituents. Such fast deactivation processes preclude both the use of Ni-catalyzed oligomerization for larger alkenes and the assessment of mechanistic aspects of the elementary steps that mediate dimerization turnovers. The identity and kinetic relevance of such steps remain the subject of active inquiry and controversy [30–39], with proposed mechanisms predominantly based on analogies between homogeneous complexes and Ni-based aluminosilicates, in spite of their distinct reactivity and co-catalyst requirements.

The capillary condensation of ethene reactants as an extended liquid phase within Ni-Al-MCM-41 mesopores led to very high dimerization turnover rates (per Ni atom), to high selectivity to primary dimers, and to nearly undetectable deactivation at sub-ambient temperatures (230–250 K) [28]. Ethene dimerization turnover rates were much higher than on previously reported Ni-based aluminosilicates, in spite of the much higher temperatures used in previous studies (>350 K) [22–27]. The strong effects of intrapore liquids were attributed to the selective enhancement of the desorption rates of bound dimers, through the preferential solvation of their late desorption transition states, which resemble a nearly-detached 1-butene molecule immersed within the contacting intrapore non-polar liquids. These enhanced desorption rates inhibit the secondary growth and isomerization of these bound species during their initial formative sojourn. The stability of Ni active sites within liquid-filled channels allows detailed rate and kinetic measurements, as well as the conclusive identification of the active centers as grafted (Ni-OH)⁺ sites, which form during synthesis via the stoichiometric exchange of isolated protons in Al-MCM-41 by aqueous solutions of Ni²⁺ cations.

These concepts and mechanistic insights represent, in fact, a general feature of alkene dimerization catalysis, as shown here for propene and butene reactants, for which deactivation in the absence of intrapore liquids is even faster than for ethene [28,40–42]. The stable rates and the very high selectivity to primary dimers when liquids form within Ni-Al-MCM-41 channels render Ni-catalyzed dimerization of larger alkenes potentially practical. Propene and butene dimerize with very high turnover rates at sub-ambient temperatures (230–250 K) and without detectable deactivation at conditions that coincide with their respective condensation points within Ni-Al-MCM-41 channels with 1.7 or 3.5 nm mean diameters.

Such remarkable stability and dimer selectivities are also evident when the condensed liquids contain unreactive alkanes, indicating that these solvation effects reflect non-specific van der Waals interactions that do not require specific chemical functionalities or molecular motifs. These findings make the choice of non-polar condensed phase one of convenience, based on volatility, purity, and inert character, without restricting the choices to the specific pressures or temperatures required for the condensation of any given alkene reactant.

Dimerization rates (per mass) for all alkenes reach their highest values when one Ni²⁺ replaces each of H⁺ initially present in Al-MCM-41, consistent with the sole involvement of isolated (Ni-OH)⁺ species in dimerization turnovers, as shown earlier for the specific case of ethene reactants [28]. The equilibrium constants for alkene binding and the rate constant for C–C bond formation steps increase markedly with reactant size. These rate constants reflect the Gibbs free energies of formation of the C–C coupling transition state (TS) from two gaseous alkene reactants. Its enthalpic component reflects a combination of the interactions between

TS structures with (Ni-OH)⁺ sites and with MCM-41 channel walls. Preliminary theoretical assessments suggest that dimerization reactions are not mediated by cationic TS structures, consistent with (Ni-OH)⁺ species that are much weaker Brønsted acids than O-H groups in aluminosilicates; such TS structures are likely to involve concerted interactions with acid-base site pairs in grafted (Ni-OH)⁺. Measured activation entropies are nearly consistent with those calculated for TS structures that resemble the bound dimer products, consistent with the weak solvent effects of intrapore liquids on the transition state for the kinetically-relevant C–C dimerization steps.

2. Methods

2.1. Synthesis of Ni-Al-MCM-41 catalysts

Ni-Al-MCM-41 samples (0.1–8.0% wt. Ni, 0.1–8.0 Ni²⁺:H₀⁺ atomic ratio, H₀⁺ defined as the concentration of H⁺ in Al-MCM-41 before Ni²⁺ exchange; H₀⁺ quantified as described in Section 2.2) were prepared by contacting solutions of 0.01–0.5 M Ni(NO₃)₂·6H₂O (99.9%, Sigma-Aldrich) in deionized water (resistivity ≈ 0.06 μS cm⁻¹) with Al-MCM-41 powders (Si/Al = 40, Sigma-Aldrich, 1.8·10⁻⁴ mol H₀⁺ g⁻¹) with small cylindrical channels (1.7 ± 0.5 nm diameter, assessed from N₂ uptakes, Section 2.4). These suspensions (pH = 3.3–3.7) were stirred for 24 h in a round-bottom flask held at 353 K. The solids were recovered by filtration, rinsed with deionized water (5 L g⁻¹), and treated in ambient air at 393 K for 12 h and then in flowing air (ultra dry, Praxair, 0.5 cm³ g⁻¹ s⁻¹) at 823 K (0.083 K s⁻¹) for 3 h. This protocol resulted in Ni-Al-MCM-41 samples with Ni²⁺:H₀⁺ ratios less than unity. An analogous protocol without the rinsing step resulted in Ni-Al-MCM-41 samples with Ni²⁺:H₀⁺ ratios greater than unity.

A Ni-Al-MCM-41 sample with larger channels (3.5 ± 2.5 nm diameter, assessed from N₂ uptakes, Section 2.4) and a broader pore-size distribution (Fig. S7, SI) was prepared using Al-MCM-41 samples synthesized using reported protocols [43]. A mixture of sodium silicate (28.7% wt. silica, 18.7 g, Sigma-Aldrich), Al(NO₃)₃ (0.1 g, 99.9%, Sigma-Aldrich) and sulfuric acid (10 mL, 1.2 M) in deionized water (resistivity ≈ 0.06 μS cm⁻¹, 40 g) was mixed with an aqueous solution of cetyltrimethylammonium bromide surfactants ((C₁₆H₃₃)N(CH₃)₃Br, 50 mL, 0.05 M, >99%, Sigma-Aldrich) by stirring for 0.5 h at ambient temperature. The resulting mixture was placed within a Teflon-lined autoclave and treated at 373 K under autogenous pressure for 72 h. The solids were recovered by filtration, rinsed with deionized water (5 L g⁻¹), treated in ambient air at 393 K for 12 h, and then in flowing air (ultra dry, Praxair; 0.5 cm³ g⁻¹ s⁻¹) by heating to 873 K at 0.083 K s⁻¹ and holding for 3 h. The protons in this large-pore Al-MCM-41 sample were exchanged with Ni cations using the same procedures as described above for the small-pore Ni-Al-MCM-41, resulting in Ni contents (0.3% wt.) corresponding to a Ni²⁺:H₀⁺ ratio of 0.6 in this large-pore Ni-Al-MCM-41 sample.

2.2. Titration of accessible protons in Al-MCM-41

The number of protons in Al-MCM-41 samples (1.7 and 3.5 nm mean pore diameter) before Ni exchange (H₀⁺) was measured using 2,6-di-*tert*-butylpyridine (DTBP, >97%, Sigma-Aldrich) as a selective titrant of Brønsted acid sites [44]. Al-MCM-41 samples were, prior to titration with DTBP, subjected to the protocol identical to that used to prepare Ni-Al-MCM-41 samples (Section 2.1) except that aqueous solutions of HNO₃ (Sigma-Aldrich, 70%, AR grade), instead of aqueous solutions of Ni(NO₃)₂·6H₂O, were contacted with Al-MCM-41 at pH values matching that used during preparation of Ni-Al-MCM-41 (pH = 3.3–3.7). The titration was performed

by contacting DTBP (0.05 kPa, 0.01 mol_{DTBP} g⁻¹ h⁻¹) over a fixed-bed of Al-MCM-41 aggregates at 448 K using reaction protocols described in Section 2.3. A solution of DTBP in *n*-hexane (99%, Sigma-Aldrich; 1:25 DTBP:*n*-hexane molar ratio) was delivered using a syringe pump (Cole-Parmer, 60061 series) and vaporized into a He stream. The concentration of DTBP in reactor influent and effluent mixtures was determined using chromatographic protocols described in Section 2.3, and H₀⁺ values were assessed by assuming unit stoichiometry between adsorbed DTBP and H⁺ [6].

2.3. Alkene dimerization rate and selectivity measurements

Dimerization rates of ethene (99.999%, Praxair), propene (99.9%, Praxair), and 1-butene (99.5%, Praxair) were measured on fixed-beds comprised of mixtures of Ni-Al-MCM-41 aggregates (125–180 μm) and SiO₂ aggregates (125–180 μm) supported between quartz wool plugs and held within a stainless steel tubular reactor (6.4 mm outer diameter, 316 stainless steel). Ni-Al-MCM-41 aggregates (5–15 mg) were mixed with SiO₂ aggregates (Davisil-62, Sigma-Aldrich, treated in air, 1073 K, 8 h) in 1:50 mass ratios (Ni-Al-MCM-41:SiO₂) to avoid corruptions to measured rates and selectivities arising from bed-scale temperature gradients otherwise imposed by the fast rates. 1-Butene dimerization rates were measured by placing a bed of Al-MCM-41 (Si/Al = 40, Sigma-Aldrich) above the Ni-Al-MCM-41 catalyst bed in order to remove impurities (present in the 1-butene source), which otherwise led to site blockage and extrinsic catalyst deactivation (20:1 Al-MCM-41: Ni-Al-MCM-41 mass ratio). No oligomers were detected in 1-butene reactions on Al-MCM-41 at the examined dimerization temperatures (230–250 K). Fixed-beds were treated in flowing dry air (ultra dry, Praxair; 0.5 cm³ g⁻¹ s⁻¹) by heating to 823 K (0.083 K s⁻¹, 0.5 h hold) and then in flowing He (99.999%, Praxair) before cooling to reaction temperatures (240–273 K) and introducing alkene reactants (10–20 mol g⁻¹ h⁻¹).

Inlet flow rates were metered using electronic controllers (Porter). The hydrocarbon mixtures containing alkenes (ethene, propene) and alkanes (ethane, 99.9%; propane, 99.9%, Praxair) were achieved using adjusted flows for each hydrocarbons. Temperatures were measured with a K-type thermocouple and maintained using resistive heating and electronic temperature controllers (Watlow 982). Subambient reaction temperatures were achieved by flowing cold N₂ vapor from the headspace of a liquid N₂ dewar and using resistive heating to maintain constant temperatures. Pressures were controlled electronically (LF-1, Equilibar controller). Reactant and product concentrations were measured by flame ionization detection after chromatographic separation (Agilent 6890; HP-1 methyl silicone column, 25 m, 0.32 mm diameter, 1.05 μm film thickness); retention times were determined by molecular speciation using mass spectrometry after separation with a similar chromatographic column [45].

Dimer product selectivities on a carbon basis (S_{dim}) are reported as:

$$S_{dim} = \frac{\text{amount of C atoms in dimer}}{\sum \text{amount of C atoms in each product}} \quad (1)$$

where the amount of C atoms in a given product is obtained from the measured molar concentration and the corresponding number of C atoms in each product.

Dimer product selectivities on a molar basis (S_{C2n}) are reported as:

$$S_{C2n} = \frac{\text{moles of dimer}}{\sum \text{moles in each product}} \quad (2)$$

First-order deactivation rate constants (k_d) are used to define the stability of active Ni species during dimerization:

$$\frac{r_{2n}(t)}{r_{2n}(t_0)} = \exp[-k_d(t - t_0)] \quad (3)$$

where r_{2n}(t₀) and r_{2n}(t) represent dimerization rates at an initial t₀ and at a given t time. The catalyst mean life is defined as the inverse of the first-order deactivation rate constants.

2.4. Catalyst textural properties and compositions

N₂ physisorption uptakes were measured volumetrically at its normal boiling point (ASAP 2020, Micromeritics). Ni-Al-MCM-41 samples (~50 mg) were treated at 623 K (heating rate, 0.17 K s⁻¹) for 4 h under dynamic vacuum (10⁻⁵ bar) prior to uptake measurements. Pore size distributions in Ni-Al-MCM-41 samples were determined from N₂ desorption isotherms measured at its boiling point at ambient pressure using the Barret-Joyner-Halenda (BJH) equation [48]. The translation of N₂ isotherms into the corresponding uptakes of alkene reactants within small-pore Ni-Al-MCM-41 channels at reaction temperatures is described in Section 3.2. Ni contents were measured by inductively-coupled plasma atomic emission spectrometry (ICP-AES; Galbraith Laboratories).

3. Results and discussion

3.1. Dimerization rates and selectivities using ethene, propene, and 1-butene: The consequences of intrapore liquid alkene reactants on catalyst stability

The involvement and reactivity of isolated Ni sites, present as grafted (Ni-OH)⁺ species formed by exchange of aqueous Ni²⁺ at H⁺ sites within Al-MCM-41 pores was shown by ethene dimerization rates (per mass) that were strictly proportional to the number of Ni atoms up to stoichiometric exchange levels and then remained constant at Ni²⁺:H₀⁺ ratios above unity [28]. These ratios are defined as the number of Ni²⁺ atoms in each sample per initial H⁺ (H₀⁺) in the Al-MCM-41 precursors (Section 2.1). The results presented in this Section show the strong influence of the intrapore liquids phase on the stability of Ni-Al-MCM-41 catalysts during propene and 1-butene dimerization reactions. Such stability allows, in turn, the identification of (Ni-OH)⁺ species as the sole centers of reactivity for propene and butene dimerization on Ni-Al-MCM-41, as shown by the data in Section 3.5.

Table 1 shows measured mean lives (defined in Section 2.3) on each Ni-Al-MCM-41 sample during propene and 1-butene reactions at 248 K, as well as the previously reported data for ethene reactants [28]. Table 1 also shows the results of previous studies for propene and 1-butene reactants at 353–453 K on Ni-based aluminosilicates prepared by ion-exchange or grafting of organometallic precursors [40–42]. Reported Ni-based aluminosilicates showed rapid deactivation above 350 K, conditions that lead to reactants and products that remain gaseous within mesopores. Deactivated Ni-based aluminosilicates can be reactivated by treatment in He at 723 K after ethene reactions, indicative of bound oligomers that can be detached from active sites via direct desorption, without requiring chemical reactions for their removal [28]. The alkene dimerization elementary steps (Section 3.6) that describe all dimerization rate data indicate that alkene binding on (Ni-OH)⁺ becomes stronger with increasing alkene size, consistent with the faster deactivation evident for larger alkenes. These size effects likely reflect the stronger van der Waals interactions and covalent binding expected for larger molecules on surfaces [46]. These stronger van der Waals forces are also responsible for the higher enthalpy of vaporization and boiling point of larger hydrocarbons.

Table 1
Alkene dimerization rates (per total Ni atom) and dimer selectivity on Ni-based aluminosilicates.

Alkene	Ethene		Propene		1-Butene	
Catalyst	Ni-Al-MCM-41		Ni-Al-MCM-41		Ni-Al-MCM-41	
% wt. Ni	0.2	2.0	0.2	0.6	0.2	0.6
Temperature (K)	258	448	248	453	248	353
Pressure (MPa)	2.6	3.5	0.23	0.50	0.055	0.050
Intrapore fluid phase	liquid	gas	liquid	gas	liquid	gas
Dimerization rates ($\text{mol}_{\text{alkene}} (\text{atom Ni})^{-1} \text{h}^{-1}$)	38,900	15,700	1200	480	350	160
Dimers among products (% C-basis) ^a	88 (1-C ₄) ^c	35 (1-C ₄) ^c	91 (C ₆) ^c	41 (C ₆) ^c	93 (C ₈) ^c	15 (C ₈) ^c
Alkene conversion at reported dimers %	8	1.5	5	2	3	5
Mean life (h) ^b	>600	90	>600	9	>600	4
Reference	28		This study	40, 41	This study	42

^a Selectivity on a carbon-basis, as defined by Eq. (1) (Section 2.3).

^b Mean life defined in Section 2.3; k_d values (Eq. (3), Section 2.3) are obtained from the local slope of dimerization rates (r_{2n}) as a function of time on stream.

^c 1-C₄ refers to 1-butene, and C₆ and C₈ refer to C₆ and C₈ alkene products, respectively.

Indeed, deactivation becomes much faster for larger alkenes, as evident from the shorter mean lives during propene and 1-butene (4–9 h) than ethene (90 h) reactions at temperatures (353–453 K) typically required for adequate rates on Ni-based catalysts (Table 1). Such deactivation prevails at temperatures and pressures that maintain reactants in their gaseous state within MCM-41 channels. The slower desorption of more strongly-bound larger alkenes also favors subsequent C–C bond formation events during a single surface sojourn, as shown by primary dimer selectivities that decrease markedly with increasing alkene size (Section 3.7). The faster deactivation caused by larger alkene reactants is also evident at subsambient temperatures (230–250 K) for alkene pressures below those required to form intrapore liquids. Deactivation becomes undetectable (with mean lives higher than 600 h), however, at relative alkene pressures (defined as the ratio of alkene pressure and its saturation pressure at reaction temperature) that cause the formation of an intrapore dense phase within each Ni-based mesoporous aluminosilicate for each alkene reactant (Figs. 1–4).

In this study, dimerization rates are reported as the number of alkene reactant molecules converted to dimers, irrespective of whether these dimers subsequently react along the catalyst bed

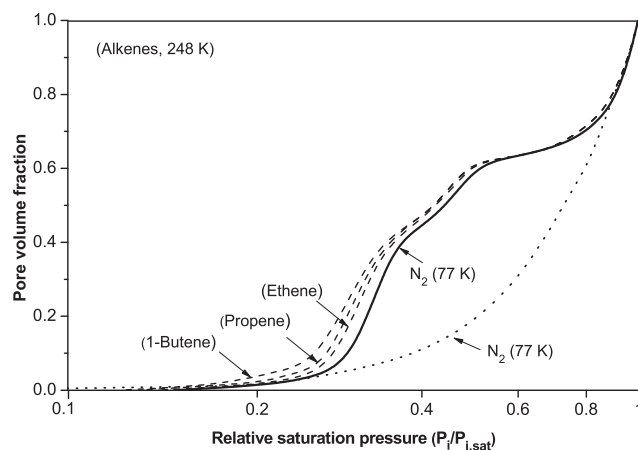


Fig. 2. Pore volume fraction for small-pore Ni-Al-MCM-41 ($\text{Ni}^{2+}:\text{H}_0^+ = 5$, pore diameter 1.7 ± 0.5 nm) filled with N_2 at 77 K (continuous line) or alkenes at 248 K (dashed lines), and for large-pore Ni-Al-MCM-41 ($\text{Ni}^{2+}:\text{H}_0^+ = 0.6$, pore diameter 3.5 ± 2.5 nm) filled with N_2 at 77 K (dotted line) as a function of the corresponding relative saturation pressure ($P_i/P_{i,\text{sat}}$). Pore volume fraction is derived from the BJH equation [48] using N_2 and C₂–C₄ alkenes as adsorbents (details in Section S2, S1). Pore size distributions shown in Fig. S7.

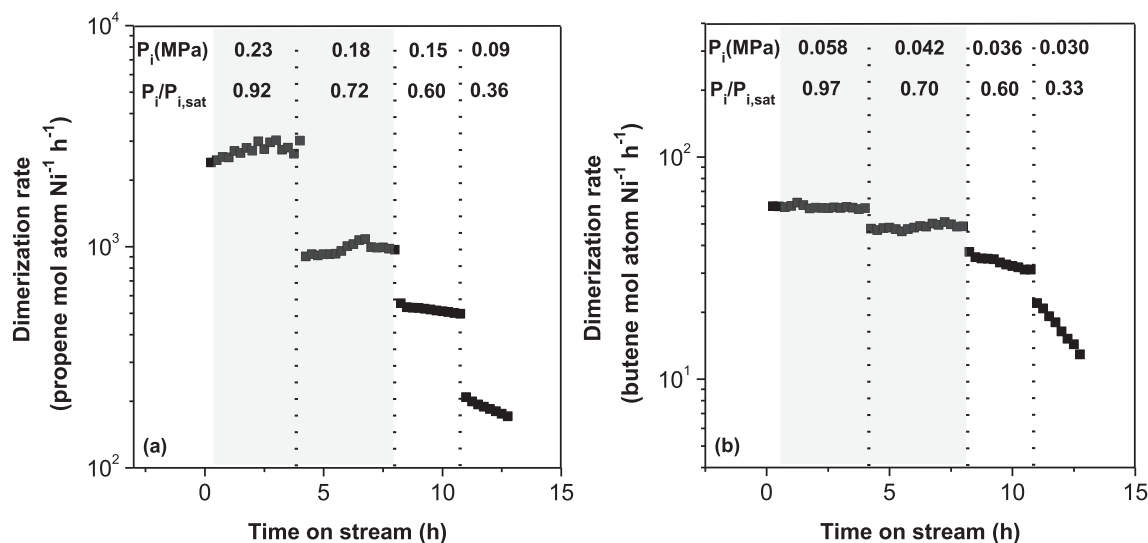


Fig. 1. Alkene dimerization rates (per active Ni) for propene (Fig. 1a) and 1-butene (Fig. 1b) at 248 K on small-pore Ni-Al-MCM-41 ($\text{Ni}^{2+}:\text{H}_0^+ = 5.0$) as a function of time on stream. P_i is alkene pressure and $P_i/P_{i,\text{sat}}$ is alkene relative saturation pressure of the corresponding alkene. Alkene pressure varied within the same experiment. Fig. 1b shows total butene dimerization rates because C₈ formation rates are independent of 1-butene/2-butene ratio. 1-Butene dimerization rates were measured using H-MCM-41 as trap for impurities at 248 K (mass ratio of 20:1H-MCM-41:Ni-Al-MCM-41); H-MCM-41 does not contribute to the formation of detectable oligomer products from 1-butene at 248 K. The shaded areas represent conditions where pores smaller than 2 nm in diameter (which constitutes 90% of the Ni-Al-MCM-41 surface area) are filled with liquid-reactants (as inferred from pore filling models, Fig. 2).

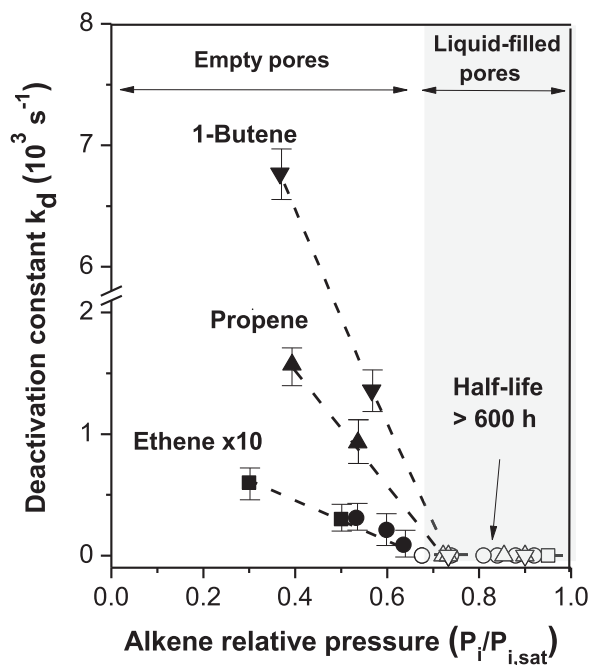


Fig. 3. First-order deactivation constants (k_d ; Eq. (3), Section 2.3) during dimerization of alkenes on small-pore Ni-Al-MCM-41 ($Ni^{2+}:H_0^+=5.0$) for ethene (rates in Fig. S1, S1, 248 K, 0.4–2.0 MPa, ●), ethene and ethane mixtures (rates in Fig. 4, 248 K, ■), propene (rates in Fig. 1a, 248 K, 0.1–0.3 MPa, ▲) and 1-butene (rates in Fig. 1b, 248 K, 0.06–0.02 MPa, ▼) as a function of the ratio of pressure to its saturation pressure ($P_i/P_{i,sat}$). Alkene conversion for all conditions remains below 10%. Shaded area corresponds to the relative pressures required to fill pores smaller than 2 nm with alkene liquids (estimated from pore filling models, Fig. 2). Dashed lines used as trend to guide the eye.

to form larger oligomers. Fig. 1 shows dimerization rates at 248 K as a function of time on stream at different alkene pressures (P_i) for propene (Fig. 1a, 0.090–0.23 MPa) and 1-butene (Fig. 1b, 0.030–

0.058 MPa) on Ni-Al-MCM-41 samples with small channels (1.7 ± 0.5 nm pore diameter). Dimerization rates become stable at propene pressures above 0.15 MPa and 1-butene pressures above 0.036 MPa (Fig. 1). Each of these threshold pressures (P_i^*) correspond to 0.60–0.65 of their respective saturation pressures ($P_{i,sat}$) at 248 K (0.25 MPa, propene; 0.060 MPa, 1-butene [47]); rates also became constant with time on stream for ethene [28] at this relative pressure ($P_i/P_{i,sat} = 0.6$; $P_{C2,sat} = 2.1$ MPa at 248 K). Such $P_i/P_{i,sat}$ ratios correspond to those required to condense each alkene within channels smaller than 2 nm in diameter in each small-pore Ni-Al-MCM-41 sample, as shown previously for ethene [28] and here in Fig. 2 for propene and butene reactants.

The data in Fig. 1 show that the temperatures and alkene pressures required for the formation of an intrapore liquid phase within Ni-Al-MCM-41 channels coincide with those that prevent the fast deactivation of active sites otherwise observed when mesopores predominantly contain reactants and products in their gaseous state. At each condition, deactivation rate constants decreased with time on stream because the concomitant decrease in reactant conversion (whether caused by deactivation or by changes in bed residence time) leads to lower prevalent oligomer concentrations, thus decreasing the extent to which they can read-sorb and grow. Higher alkene reactant pressures also increase the average chain length of the oligomerization products formed, making the abrupt stabilization observed at reactant pressure above P_i^* , as well as the counteracting effect of the intrapore liquid phase, even more remarkable. In addition to the observed stabilization of Ni-OH⁺ sites, the presence of an extended intrapore liquid phase at 248 K leads to much higher dimerization rates (per Ni atom) than previously reported on Ni-based aluminosilicates (Table 1) even at much lower temperatures than in previous reports (350–450 K) for which the lower rates likely reflect very rapid deactivation during initial contact with alkene reactants, as shown for ethene dimerization, for Ni-Al-MCM-41 at 448 K [28].

The temperatures and pressures that lead to capillary condensation also give higher selectivities to primary dimers for each alkene reactant than those for gas filled mesopores (Table 1), an

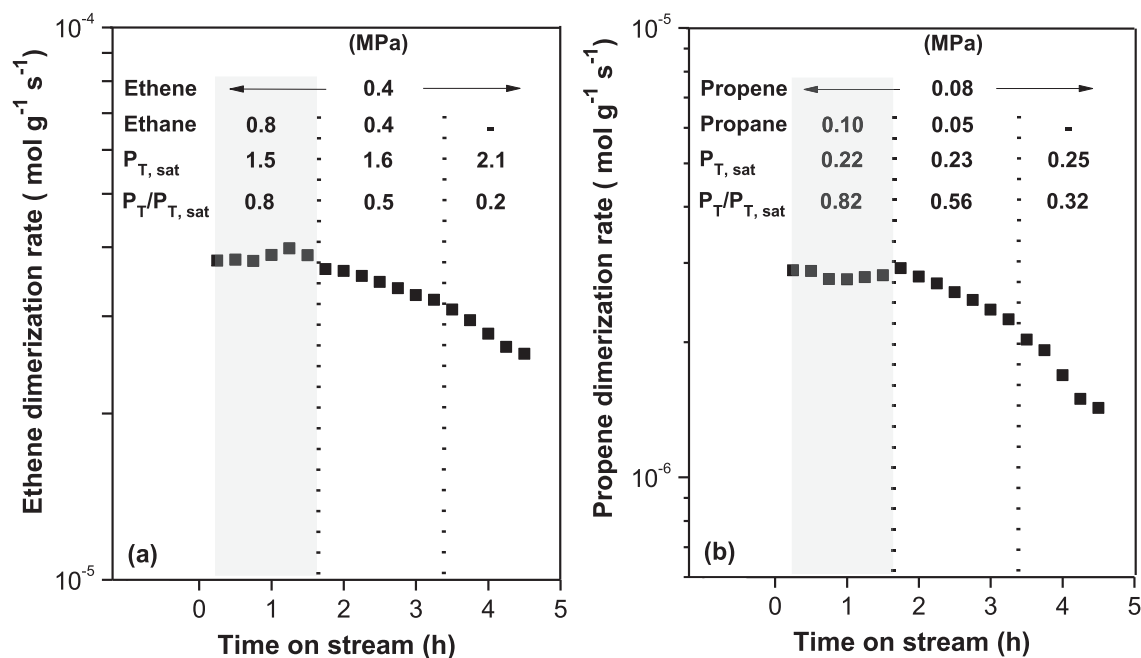


Fig. 4. Alkene dimerization rates (per mass) on small-pore Ni-Al-MCM-41 (pore diameter 1.7 ± 0.5 nm) as a function time on stream during the co-feeding of mixtures of ethene and ethane (248 K, Fig. 4a) and of propene and propane (248 K, Fig. 4b). Shaded area corresponds to conditions where pores smaller than 2 nm in diameter are liquid-filled (as inferred from Fig. 2).

indication of their more prevalent desorption before subsequent C—C bond formation events, as also found for ethene reactants [28]. The addition of another alkene monomer to the dimers formed during such initial surface sojourns can also occur via their readsorption along the catalyst bed, as evident from the effects of bed residence time on product selectivity for propene and 1-butene reactants, shown later in Section 3.7.

3.2. Relative pressures required for condensation of alkenes and alkanes within MCM-41 mesopores at reaction temperatures

The pressures and temperatures required to condense each alkene within Ni-Al-MCM-41 mesopores were determined using N_2 uptake isotherms at 77 K and the Barret-Joyner-Halenda (BJH) equation [48]. This equation combines multilayer adsorption isotherms and the Kelvin equation for capillary condensation to describe uptakes at each pressure and temperature for any given molecule based on its vapor pressure molar volume, and surface tension as a liquid. Here, measured N_2 desorption isotherms are used to calculate the pore size distribution in Ni-Al-MCM-41 (from N_2 properties at 77 K). This size distribution is then used to estimate the uptakes for each alkene from their respective properties at 248 K (Figure S2, SI). This method gives the extent to which mesopores in Ni-Al-MCM-41 are filled with a liquid phase of any given molar volume, surface tension, and saturation vapor pressure at each temperature used for dimerization catalysis. The nearly-uniform channels in these materials lead to a sharp increase in uptakes at the $P_i/P_{i,sat}$ ratios that cause condensation of a liquid phase within channels of such dimensions.

The estimated uptakes for each alkene at 248 K and for N_2 at 77 K are shown in Fig. 2 as a function of their respective relative pressures ($P_i/P_{i,sat}$) (details in S3, SI). The similarities among uptake profiles for all molecules suggest that non-specific van der Waals interactions (also responsible for the difference in vapor pressure among these molecules) account for the formation of a dense phase on flat surfaces (at $P_{i,sat}$) or within cylindrical channels of a given size (at the $P_i/P_{i,sat}$ ratios required for capillary condensation for channels of different diameters). The alkene uptakes in Fig. 2 can be used to determine the number of molecules present within MCM-41 channels at the conditions of dimerization reactions by substituting alkene surface tension and molar volume for those of N_2 in the BJH formalism (Section S3, SI). N_2 uptakes at 77 K on Ni-Al-MCM-41 thus represent accurate surrogates for the relative pressures required for uptakes and pore filling in the case of alkenes and other non-polar molecules within voids exhibiting predominantly hydrophobic surfaces.

3.3. Effects of intrapore liquids on the stability and reactivity of Ni-Al-MCM-41 catalysts

First-order deactivation rate constants (k_d ; Eq. (3), Section 2.3) are shown in Fig. 3 for all alkene reactants as a function of their respective ($P_i/P_{i,sat}$) ratios at 248 K. ($P_i/P_{i,sat}$) values above 0.60–0.65 lead to essentially undetectable deactivation and to mean catalyst lives longer than 600 h for all reactants. These mean lives become much smaller at ($P_i/P_{i,sat}$) ratios below those required to fill all MCM-41 channels. The stabilization brought forth by intrapore liquids is even more evident for propene and 1-butene reactants than for ethene; these larger alkenes condense at lower pressures and lead to faster deactivation of Ni-based catalysts than ethene when mesopores predominantly contain gaseous reactants (k_d values shown in Fig. 3; previous studies in Table 1 [40–42]). The deactivation constants were obtained under deactivating rate conditions ($P_i/P_{i,sat} < 0.6$), and given their linear trend the k_d values were indistinguishable at different time values on time-on-stream. The monotonic decrease in k_d with increasing alkene pressure

reflects the gradual filling of the smaller channels in Ni-Al-MCM-41, which represent the largest fraction of the total surface area, and the protection of the Ni sites present within such channels from deactivating events.

In contrast with the stabilization effects provided by intrapore liquid alkenes, the stability of the kinetically-relevant C—C coupling transition state is much more weakly influenced by intrapore liquids than the dimer desorption transition state, leading to second-order dimerization rate constants that do not change abruptly at the alkene reactant pressures required for intrapore condensation for ethene [28] and for propene and 1-butene reactants (as shown in Section 3.6). The mechanistic interpretations of dimerization rates for propene and 1-butene are discussed in Section 3.6 in the context of thermodynamically non-ideal conditions, which indicate that the stability of C—C coupling transition states predominantly reflect their interactions with active Ni structures and less their solvation by the intrapore liquid phase.

3.4. Dimerization rates in the presence of intrapore liquid alkenes in mixtures with alkanes or within large mesopores

The proposal that non-polar liquid alkenes within MCM-41 channels preferentially stabilize oligomer desorption transition states through non-specific van der Waals interactions indicates that other non-polar molecules would act in a similar manner. The ability of inert non-polar liquids to serve this purpose would allow the selection of appropriate inert molecules for the conditions of temperature and alkene pressures most suitable for alkene oligomerization catalysis. More specifically, inert non-polar solvents, such as alkanes, could provide the active site stabilization, inhibited deactivation, and higher primary dimer selectivities, reported here for the case of the alkene reactants also acting as the intrapore liquids.

Fig. 4 shows dimerization turnover rates for ethene (0.4 MPa ethene, Fig. 4a) and propene (0.08 MPa propene, Fig. 4b) reactants at 248 K as a function of time on stream at different pressures of ethane or propane, respectively. These pressures span a combined $P_i/P_{i,sat}$ range above and below those required for condensation within MCM-41 mesopores (0.60–0.62). Ethene and propene dimerization turnover rates remain essentially unchanged with time when combined alkane and alkene relative pressures are 0.80 for the respective alkane-alkene mixture saturation pressure ($P_{T,sat}$). These data confirm that van der Waals forces, which mediate the condensation of non-polar molecules as liquids, also account for the solvation effects that inhibit deactivation. These deactivating events reflect subsequent C—C bond formation at primary bound dimers, the desorption of which is favored by the selective solvation of their late desorption transition states by non-polar liquids.

These mechanistic inferences are consistent with the relative pressures required to inhibit deactivation in Ni-Al-MCM-41 samples with larger and less uniform channels (3.5 ± 2.5 nm diameter, pore size distribution shown in Fig. S7, SI). The filling of these larger channels occurs at higher relative pressures and leads to concomitant catalytic consequences that become evident at higher relative pressures and that emerge more gradually with increasing pressure than for Ni-Al-MCM-41 samples with smaller and more uniform channels (1.7 ± 0.5 nm diameter, Figs. 1–4). Ethene dimerization rates at 248 K on these two Ni-Al-MCM-41 samples are shown in Fig. S8 (SI). First-order deactivation constants (k_d) derived from these rate data are shown in Fig. 5 as a function of ($P_i/P_{i,sat}$) ratios for ethene reactants on these two Ni-Al-MCM-41 catalysts. Fig. 5 shows that larger mesopores require higher $P_i/P_{i,sat}$ ratios for stability and that k_d values decrease more gradually as $P_i/P_{i,sat}$ ratios increase, because pore filling occurs at higher pres-

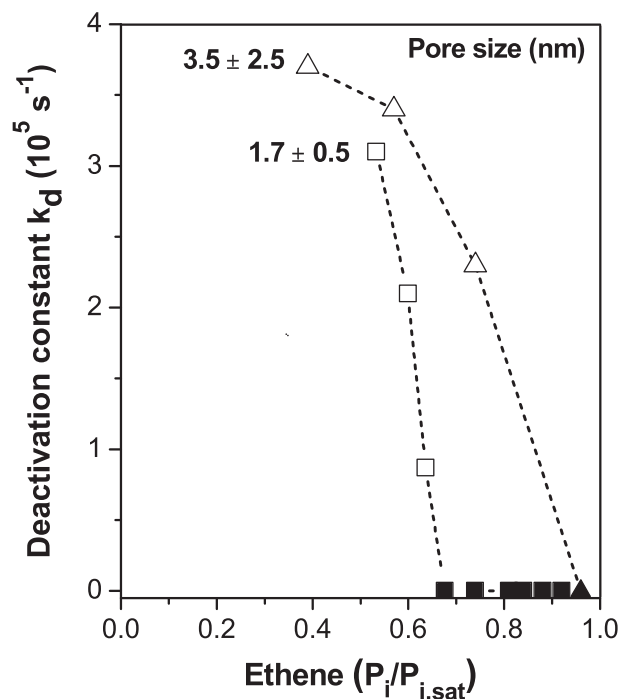


Fig. 5. First-order deactivation rate constants (k_d , Eq. (3), Section 2.3) for small-pore Ni-Al-MCM-41 (1.7 ± 0.5 nm, $\text{Ni}^{2+}:\text{H}_0^+ = 5.0$, \square , \blacksquare) and large-pore Ni-Al-MCM-41 (3.5 ± 2.5 nm, $\text{Ni}^{2+}:\text{H}_0^+ = 0.6$, Δ , \blacktriangle) as a function of the ratio of ethene pressure to its saturation pressure ($P_i/P_{i,\text{sat}}$). The k_d values were obtained from local slopes of rate data versus time on stream for small-pore (Fig. S8a) and large-pore (Fig. S8b) Ni-Al-MCM-41 samples. Filled symbols refer to pores filled with liquid ethene and empty symbols to pores filled with gaseous ethene. Dashed lines shown to guide the eye.

pressures and over a broader range of pressure, as also evident from N_2 uptake isotherms (77 K; Fig. 2).

3.5. Effects of Ni content on dimerization rates and the role of isolated $(\text{Ni-OH})^+$ species as active centers

The remarkable stability of these Ni-Al-MCM-41 catalysts with ethene, propene, and butene reactants allows systematic and accurate inquiries into the nature of the required active sites and a systematic assessment of the elementary steps responsible for dimerization turnovers, as shown next for $\text{C}_2\text{-C}_4$ alkenes in Section 3.6.

Ethene, propene, and 1-butene dimerization rates were measured on small-pore Ni-MCM-41 samples with different Ni contents. These samples were prepared by replacing some or all the protons (H^+) initially present in Al-MCM-41 (H_0^+) with Ni^{2+} cations ($\text{Ni}^{2+}:\text{H}_0^+ = 0.1\text{-}8.0$) using the procedures described in Section 2.1. Ethene dimerization rates (per mass) increased linearly with Ni content up to $\text{Ni}^{2+}:\text{H}_0^+$ ratios of unity and then remained constant for higher Ni contents [28]. These linear trends for ethene and the constant rates achieved at such a stoichiometry are consistent with the involvement of $(\text{Ni-OH})^+$ as the sole active centers, exchanged at isolated H^+ sites initially present in Al-MCM-41, and the full titration of H^+ sites when $\text{Ni}^{2+}:\text{H}_0^+$ is unity. Ni^{2+} species bridging two grafting sites ((Ni-O-Ni^{2+})) cannot account for this exchange stoichiometry in light of the very low H^+ density in the Al-MCM-41 precursor ($0.1 \text{ H}^+ \text{ nm}^{-2}$, H^+ site quantification described in Section 2.2).

The trends with Ni content and the saturation exchange stoichiometries reported for ethene are also observed for propene and 1-butene reactants. Fig. 6 shows ethene, propene and 1-butene dimerization rates (per Ni present in Ni-Al-MCM-41;

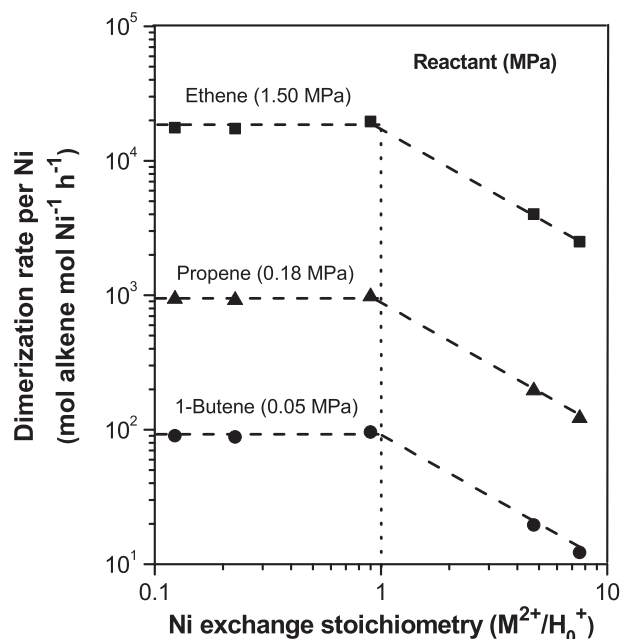


Fig. 6. Dimerization rates (per total Ni, quantification described in Section 2.4) at 248 K for ethene (1.50 MPa, \blacksquare), propene (0.18 MPa, \blacktriangle) and 1-butene (0.05 MPa, \bullet) reactants as a function of $\text{Ni}^{2+}:\text{H}_0^+$ atomic ratio on small-pore Ni-Al-MCM-41 (pore diameter 1.7 ± 0.5 nm). Rates were measured at conditions (248 K, $P_i/P_{i,\text{sat}} = 0.7\text{-}0.9$) where the small-pore Ni-Al-MCM-41 channels are filled with liquid reactants. $\text{Ni}^{2+}:\text{H}_0^+$ atomic ratio calculated based on initial H^+ content (H_0^+) on Al-MCM-41 ($1.8 \cdot 10^{-4} \text{ mol H}_0^+ \text{ g}^{-1}$), determined from titration of H^+ with 2,6 di-*tert*-butylpyridine (Section 2.2). Dashed line used to guide the eye.

248 K, $P_i/P_{i,\text{sat}} = 0.7\text{-}0.9$) as a function of $\text{Ni}^{2+}:\text{H}_0^+$ ratios on small-pore Al-MCM-41 samples. All turnover rates show a constant value up to $\text{Ni}^{2+}:\text{H}_0^+$ ratios of unity and then decrease for larger $\text{Ni}^{2+}:\text{H}_0^+$ ratios, indicating that excess Ni cations do not contribute to measured rates, apparently because they exist as NiO oligomers that act as unreactive spectators. Grafted $(\text{Ni-OH})^+$ monomers, the only Ni^{2+} species able to fully titrate isolated H^+ species with a 1:1 stoichiometry (Fig. S4, SI), act as the sole active centers in dimerization turnovers for all alkene reactants.

Dimerization rates at any given $\text{Ni}^{2+}:\text{H}_0^+$ ratio (Fig. 6) are higher for ethene (1.50 MPa) than for propene (0.18 MPa) or 1-butene (0.04 MPa) reactants. These higher rates for ethene solely reflect the differences in alkene reactant pressure; rigorous kinetic analyses of these rates under thermodynamically non-ideal conditions (described in detail in Section 3.6) indicate that second-order rate constants (α' , per active $(\text{Ni-OH})^+$) increase with alkene size ($1.30 \text{ mol Ni}^{-1} \text{ s}^{-1} \text{ MPa}^{-2}$ for ethene, $7.10 \text{ mol Ni}^{-1} \text{ s}^{-1} \text{ MPa}^{-2}$ for propene, $142.8 \text{ mol Ni}^{-1} \text{ s}^{-1} \text{ MPa}^{-2}$ for 1-butene; Table 2). Dimerization rate constants (per H^+) for $\text{C}_2\text{-C}_4$ alkenes on solid Brønsted acids (H^+) at temperatures higher than 400 K also increase with alkene size [6]. The protons of the parent Al-MCM-41, however, contribute negligibly to dimerization rates at 248 K; this is also the case for residual protons in Ni-Al-MCM-41 on samples that contain $(\text{Ni-OH})^+$ sites, as evident from the constant turnover rates (per Ni) for samples that contain non-exchanged H^+ sites ($\text{Ni}^{2+}:\text{H}_0^+$ below unity, Fig. 6).

Preliminary studies using density functional theory suggest that these $(\text{Ni-OH})^+$ sites are very weak Brønsted acids, but they can catalyze ethene dimerization turnovers with very low barriers through the involvement of the O-H moiety as a Lewis acid-base pair. Their identity, presence, structure, acid-base properties, and catalytic involvement were recently proposed for ethene dimerization [28], but not previously for dimerization catalysis on other Ni-based aluminosilicates, metal-organic frameworks or

Table 2

Alkene dimerization constants (per active site) and adsorption constants (also shown in Fig. S11, SI) for small-pore Ni-Al-MCM-41 ((Ni-OH)⁺ active sites, Ni²⁺:H₀⁺ = 5.0) at 248 K, obtained through the linearization of rates (Fig. 7, Eq. (13)) and for mesoporous aluminosilicate solid acids (H⁺ active sites) at 503 K [6].

	Alkene	Ethene	Propene	1-Butene
248 K	Fugacity ^a (MPa)	1.2–1.6	0.12–0.18	0.02–0.06
	Fugacity-coefficient ^a	0.77–0.83	0.95–0.96	0.97–0.98
Site: (Ni-OH) ⁺ 248 K	α' (mol Ni ⁻¹ s ⁻¹ MPa ⁻²)	1.30 ± 0.09	7.10 ± 0.28	142.8 ± 5.7
	β' (MPa ⁻¹)	<0.5 ^b	5.0 ± 1.1	368 ± 31
	ΔH [‡] (kJ mol ⁻¹)	46 ± 5	29 ± 4	21 ± 2
	ΔS [‡] (J mol ⁻¹ K ⁻¹)	-103 ± 8	-145 ± 9	-187 ± 8
Site: H ⁺ 503 K [6] ^c	α (mol H ⁻¹ s ⁻¹ MPa ⁻²) ^d	0.002 ± 0.0005	0.014 ± 0.004	0.710 ± 0.100
	β (MPa ⁻¹) ^d	27.0 ± 0.2	95.0 ± 3.0	1357 ± 203

^a Alkene fugacity (f_n) is related to alkene pressure (P_n) through Φ_n . Alkene fugacity coefficient (Φ_n) calculated using compressibility factors (Eq. S6, SI) from generalized charts for pure gases [52].

^b β' value smaller than uncertainty.

^c Number of active H⁺ sites measured using selective titrants (DTBP) during dimerization.

^d Φ_n for H⁺ is unity at 503 K, so f_n values are equal to P_n values at 503 K.

organometallic complexes. It seems plausible that co-catalysts and activators, such as aluminoxanes, could lead to bound ligands at Ni centers and that such moieties may confer the acid-base properties required for catalysis, thus rendering such additives essential for low-temperature reactivity in Ni-based organometallic complexes [16] and metal-organic frameworks [19].

3.6. Effects of alkene size on the binding of intermediates and the stability of the kinetically-relevant C–C formation transition states on Ni-Al-MCM-41 catalysts

The effects of alkene pressure on dimerization rates are examined here for ethene, propene, and 1-butene and interpreted in the context of the kinetic relevance of bound species and elementary steps using transition state theory (TST) to describe the rate and equilibrium constants for elementary steps. Such treatments require accounting for the fugacity and activity of molecules that may exist in their thermodynamically non-ideal states at conditions near their condensation point and for the nature of transition states (TS) bound at (Ni-OH)⁺ active centers and interacting with intrapore liquids via van der Waals forces [28].

The strictly second-order dependence of rates on ethene pressure at operating conditions at 248 K indicated that bound (Ni-OH)⁺ centers remain essentially bare during steady-state ethene dimerization catalysis and that bimolecular C–C bond formation steps limit dimerization rates [28]. Propene and 1-butene reactants, however, bind more strongly at (Ni-OH)⁺ centers and lead to more complex rate equations because of the kinetically-detectable coverages of alkene-derived bound species. As a result, rate equations for propene and 1-butene must account for such coverages through denominator terms that reflect their respective binding constants. Their more complex functional forms, however, allow the measurement of such binding constants for propene and 1-butene and serve to confirm the sequence of elementary steps and the nature and role of the species bound at (Ni-OH)⁺ centers proposed earlier for ethene reactants.

Scheme 1 depicts a sequence of elementary steps that is consistent with the observed effects of pressure on alkene (C_n , $n = 2, 3, 4$) dimerization turnover rates on (Ni-OH)⁺ centers (*). These steps include vapour-liquid equilibration of reactants and products (K_C , alkene condensation constant), reactant adsorption (K_A) and desorption (K_D), and irreversible formation of the new C–C bond via reaction of an alkene in the liquid phase ($C_n(l)$) with a bound analog (C_n^*) (k_1 , alkene dimerization constant) to form the dimer product (C_{2n}^*). These C_{2n}^* species can (i) desorb (k_{D1}) to form a vacant (Ni-OH)⁺ site and a dimer in the liquid phase through the dimer desorption transition state (C_{2nD}^\ddagger) or (ii) react with an alkene reactant ($C_n(l)$) to form a bound trimer (C_{3n}^* ; k'_1 , chain-growth con-

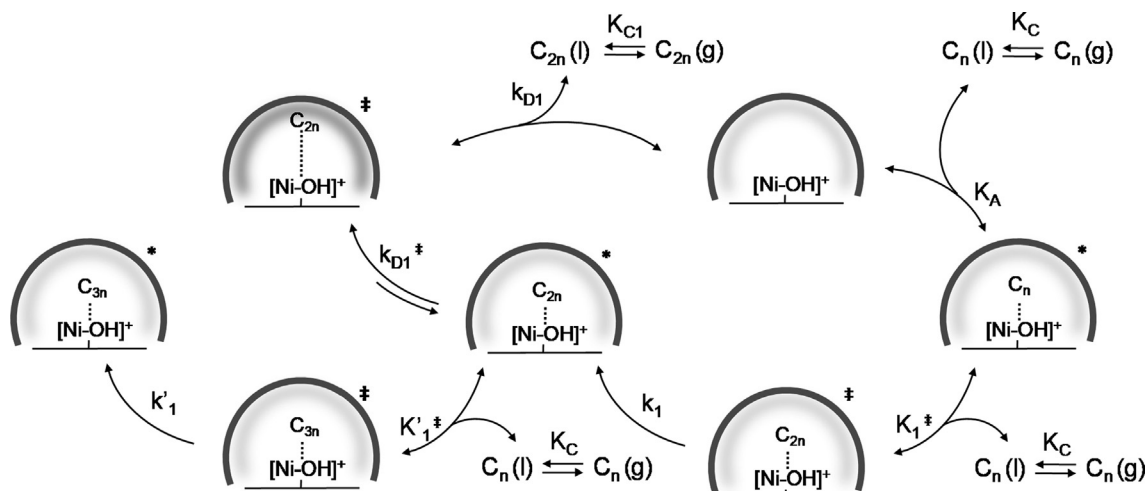
stant) through a trimer transition state (C_{3n}^\ddagger). The desorbed dimers can also readsorb to re-form C_{2n}^* species via C_{2nD}^\ddagger , thus affording an additional chance to form C_{3n}^* species in secondary surface visits.

The tenets of transition state theory [52–51] invoke equilibration between an activated complex and its precursors in an elementary step and the infrequent decomposition of this complex with a frequency given by the molecular vibration that causes the products to form, in this case the symmetric stretch of the C–C bond that is formed between two alkenes at the bimolecular TS. The concentration of the kinetically-relevant bound dimer TS is then given by (details in Eqs. S8–S19, SI):

$$[TS] = \frac{K_1^\ddagger K_A (K_C)^2 [*] (f_n)^2}{\gamma_1^\ddagger} \quad (4)$$

where K_1^\ddagger is the equilibrium constant for the formation of the C–C bond in the dimer at the TS (\ddagger), f_n is the fugacity of the gaseous alkene monomer (related to the alkene pressure (P_n) by the fugacity coefficient (Φ_n , Eq. S6, SI) [53]), $[*]$ is concentration of vacant sites and γ_1^\ddagger is the thermodynamic activity coefficient of the bound bimolecular TS. The magnitude of the TS activity coefficients may depend on the presence and identity of a liquid phase, depending on the extent to which such bound species sense the surrounding environments. Such activity coefficients become particularly sensitive to the nature of the surrounding phase when they involve reactants or products that reside within such a phase and the transition states are early or late, respectively, along the reaction coordinate [52,53]. In this study, the isolated nature of the (Ni-OH)⁺ binding sites and thus of any bimolecular transition states ([TS]; Eq. (4)) renders γ_1^\ddagger independent of the concentration of such transition states, but its magnitude can depend on the identity and on the presence or absence of a contacting liquids phase. Such solvation effects are expected to be minimal when MCM-41 channels predominantly contain gaseous species; the absence of any abrupt changes in the second-order ethene dimerization rate constants upon the abrupt formation of intrapore ethene liquids [28] indicates that such transition states are predominantly stabilized by interactions with (Ni-OH)⁺ centers and essentially insensitive to the presence of a dense contacting phase, consistent with the bound reactants and products of the C–C bond formation elementary step.

The desorption of bound dimers is an endothermic step, for which transition states (C_{2nD}^\ddagger) typically occur late along the reaction coordinate and tend to resemble the products. These products reside within the surrounding fluid and their solvation by a non-polar liquid is also felt at the transition state. The consequent faster desorption of bound dimers leads to a lower probability of subsequent growth during the initial surface sojourn that forms them,



Scheme 1. Alkene (C_n , $n = 2, 3, 4$) dimerization elementary steps on active $(\text{Ni-OH})^+$ sites for the formation of dimer products in the presence of intrapore liquid alkenes or chain-growth reactions to larger oligomers.

leading to higher single-sojourn dimer selectivities at conditions that form intrapore liquids (at zero alkene conversion, Fig. 10, Section 3.7). These data indicate that the concentration of dimer desorption transition states (C_{2n}^{\ddagger}) increases in the presence of a contacting liquid phase because solvation effects lead to smaller values of its activity coefficient (γ_{D1}^{\ddagger}).

The bimolecular bound TS complex excludes in its partition function the vibrational mode along the C–C bond being formed, because, when extracted from its full partition function, it cancels the vibrational frequency that causes the decomposition of the TS [51], leading to a dimerization rate (r_{2n}) that depends on the alkene fugacity (f_n), or its fugacity coefficient (Φ_n) and pressure (P_n) (details in Eqs. S8–S19, SI):

$$r_{2n} = \frac{\frac{k_B T}{h} K_1^{\ddagger} K_A (K_C)^2 \frac{\gamma_n^*}{\gamma_1^{\ddagger}} (f_n)^2}{1 + \frac{\gamma_n^*}{\gamma_n} (K_A K_C) f_n} = \frac{\frac{k_B T}{h} K_1^{\ddagger} K_A (K_C)^2 \frac{\gamma_n^* (\Phi_n)^2}{\gamma_1^{\ddagger}} (P_n)^2}{1 + \frac{\gamma_n^*}{\gamma_n} (K_A K_C \Phi_n) P_n} \quad (5)$$

Here, k_B is the Boltzmann constant, h is the Planck constant, T is temperature, and γ^* and γ_n^* are the activity coefficients of active $(\text{Ni-OH})^+$ sites and of bound monomers, respectively. The $K_1^{\ddagger} K_A (K_C)^2$ term is determined by the Gibbs free energy of formation of the C–C bond TS (ΔG_1^{\ddagger}), given by the free energy difference between this TS ($\Delta G^{\ddagger,0}$) and two gas-phase alkene molecules ($2\Delta G_n^0(\text{g})$), each in their thermodynamically ideal state:

$$\Delta G_1^{\ddagger} = \Delta G^{\ddagger,0} - 2\Delta G_n^0(\text{g}) \quad (6)$$

The $(\Phi_n)^2$, γ_1^{\ddagger} , γ^* and γ_n^* terms in Eq. (5) account for any thermodynamic non-ideality for molecules near their condensation point or bound at active sites. These non-idealities are captured by the excess Gibbs free energy (ΔG_E) [52] of formation of the TS from two alkene reactants in the gas-phase:

$$\Delta G_E = -RT \ln \left(\frac{\gamma^* (\Phi_n)^2}{\gamma_1^{\ddagger}} \right) \quad (7)$$

The dimerization rates are then given by:

$$r_{2n} = \frac{\frac{k_B T}{h} \exp\left(\frac{-\Delta G_1^{\ddagger}}{RT}\right) (P_n)^2}{1 + \frac{\gamma_n^*}{\gamma_n} (K_A K_C \Phi_n) P_n} = \frac{\frac{k_B T}{h} \left(\exp\left(\frac{-\Delta G_1^{\ddagger}}{RT}\right) \exp\left(\frac{-\Delta G_E}{RT}\right) \right) (P_n)^2}{1 + \frac{\gamma_n^*}{\gamma_n} (K_A K_C \Phi_n) P_n} = \frac{\alpha (P_n)^2}{1 + \beta P_n} \quad (8)$$

$$\alpha = \frac{k_B T}{h} \exp\left(\frac{-\Delta G^{\ddagger}}{RT}\right) = \frac{k_B T}{h} K_1^{\ddagger} K_A (K_C)^2 \frac{\gamma^* (\Phi_n)^2}{\gamma_1^{\ddagger}} \quad (9)$$

$$\beta = \frac{\gamma_n^*}{\gamma_n} K_A K_C \Phi_n \quad (10)$$

The parameter α represents the second-order alkene dimerization rate constant per active $(\text{Ni-OH})^+$ site, β is the equilibrium adsorption constant for the bound alkene, ΔG^{\ddagger} is the free energy of formation of dimerization TS from two gaseous alkene reactants. From the ideal (I) and excess (E) components of ΔG^{\ddagger} in Eq. (8), the ΔG^{\ddagger} term in α (Eq. (9)) can be separated into its enthalpic and entropic components:

$$\alpha = \frac{k_B T}{h} \exp\left(\frac{-(\Delta H_1^{\ddagger} + \Delta H_E^{\ddagger})}{RT}\right) \exp\left(\frac{\Delta S_1^{\ddagger} + \Delta S_E^{\ddagger}}{R}\right) \quad (11)$$

where ΔH^{\ddagger} and ΔS^{\ddagger} terms correspond to the ideal or excess enthalpy and entropy in ΔG^{\ddagger} .

The presence of intrapore liquids at 248 K shows a marked influence on the selectivity of dimer products in the first surface sojourn for all alkene reactants, as later shown in Fig. 10 (Section 3.7) by relative rates between bound dimer (C_{2n}^*) chain growth and desorption that decrease under thermodynamically non-ideal conditions (248 K, intrapore liquids) versus gaseous conditions (448 K) (relative rates evaluated at zero conversion). These relative rates depend on the stability of their respective TS structures, while any effects of a liquid phase would reflect the extent to which they are solvated by a contacting liquid phase. The ratio (χ) between the rates for C_{2n}^* growth (r_{3n}) and desorption (r_{des}) is given by:

$$\chi = \frac{r_{3n}}{r_{des}} = \frac{\frac{k_B T}{h} K_1^{\ddagger} K_C \frac{\gamma_{C_{2n}}^*}{\gamma_1^{\ddagger}} [C_{2n}] f_n}{\frac{k_B T}{h} k_{D1}^{\ddagger} \frac{\gamma_{C_{2n}}^*}{\gamma_{D1}^{\ddagger}} [C_{2n}]} = \frac{K_1^{\ddagger} K_C}{\gamma_1^{\ddagger}} \frac{f_n}{\gamma_{D1}^{\ddagger}} \quad (12)$$

In this equation, $\gamma_{C_{2n}}^*$ is the activity coefficient for bound dimers (C_{2n}^*), γ_{D1}^{\ddagger} is the activity coefficient for C_{2n}^* desorption TS (C_{2n}^{\ddagger}), k_{D1}^{\ddagger} is C_{2n}^{\ddagger} desorption constant, γ_1^{\ddagger} is the activity coefficient for C–C bond formation TS from C_{2n}^* , and $[C_{2n}^*]$ is bound dimer concentration. The activity coefficient terms in Equation (12) are related in Section 3.7 to the dimer selectivity data (Fig. 10).

Dimerization turnover rates (per $(\text{Ni-OH})^+$ site) for ethene, propene and 1-butene reactants on small-pore Ni-Al-MCM-41 are

shown in Fig. 7 at 248 K as a function of alkene fugacity using a linearized version of Eq. (5) (Eq. (13)). In this linearization, the activity coefficients of C–C bond dimer formation TS ($\gamma_{\ddagger}^{\ddagger}$), of active (Ni-OH)⁺ sites (γ^*) and of bound species (γ_n^*) are assumed to be unaffected by the presence of a liquid phase and remain unchanged with alkene pressure. The data in Fig. 7 show the expected linear trends from Eq. (13). The trends in Fig. 7 show intercepts and slopes corresponding to the second-order dimerization rate constant (α' , per active (Ni-OH)⁺ site) and the equilibrium adsorption constants (β'), respectively:

$$\frac{(f_n)^2}{r_{2n}} = \frac{h}{k_B T} \left(\frac{1}{\alpha'} + \frac{\beta'}{\alpha' f_n} \right) \quad (13)$$

$$\alpha' = \frac{k_B T}{h} K_1^\ddagger K_A (K_C)^2 \quad (14)$$

$$\beta' = K_A K_C \quad (15)$$

Table 2 shows the regressed values of α' and β' for ethene, propene and 1-butene reactants (small-pore Ni-Al-MCM-4; Ni²⁺:H₀⁺ = 5.0; 248 K). The α' values increase with alkene size, a reflection of a concomitant decrease in the Gibbs free energies of formation of the C–C coupling TS from two gaseous alkenes ($\Delta G_{\ddagger}^\ddagger$). The β' term reflects the Gibbs free energies of binding of gaseous alkenes. The β' value for ethene is too small for detection ($\beta' \ll 0.5 \text{ MPa}^{-1}$, Fig. 7; $K_A K_C f_n \ll 1$ in Eq. (5)), consistent with (Ni-OH)⁺ centers that remain essentially uncovered during catalysis and with the weak binding of ethene on such active sites, which lead to low coverages even at sub-ambient temperatures. These β' values increase with increasing alkene size ($5.0 \pm 1.1 \text{ MPa}^{-1}$, propene; $368 \pm 31 \text{ MPa}^{-1}$, 1-butene; 248 K, Table 2) and are much smaller than their respective values on Brønsted acids (H⁺) even at higher temperatures (Al-MCM-41; 503 K) (Table 2), another indication of

the weaker binding and the less negative adsorption enthalpies on (Ni-OH)⁺ centers than on aluminosilicate Brønsted acids. Such strong differences in binding are indicative of (Ni-OH)⁺ centers that interact with alkenes in a very different manner than through the formation of bound alkoxides by proton transfer in aluminosilicates. These observations seem to preclude the involvement of ion-pair transition states that mediate alkene dimerization on solid Brønsted acids [6] in dimerization catalysis on Ni-Al-MCM-41.

The effects of temperature on the magnitudes of α' and β' reflect the enthalpy and entropy components of the formation free energy of the C–C coupling transition state ($\Delta H_{\ddagger}^\ddagger$, $\Delta S_{\ddagger}^\ddagger$) from two gaseous alkenes and of the bound alkene from its gaseous precursor, respectively. The α' values (per (Ni-OH)⁺ site) are shown in Arrhenius form in Fig. 8 (233–255 K); these data can be regressed to the functional form of Equation (11) to estimate $\Delta H_{\ddagger}^\ddagger$ and $\Delta S_{\ddagger}^\ddagger$. The $\Delta H_{\ddagger}^\ddagger$ values are $46 \pm 5 \text{ kJ mol}^{-1}$ for ethene, $29 \pm 4 \text{ kJ mol}^{-1}$ for propene and $21 \pm 2 \text{ kJ mol}^{-1}$ for 1-butene (Table 2); the $\Delta S_{\ddagger}^\ddagger$ values are $-103 \pm 8 \text{ J (mol K)}^{-1}$ for ethene, $-145 \pm 9 \text{ J (mol K)}^{-1}$ for propene, and $-187 \pm 8 \text{ J (mol K)}^{-1}$ for 1-butene.

The dimer TS species, like the alkene monomers, are expected to bind weakly at (Ni-OH)⁺ centers. $\Delta H_{\ddagger}^\ddagger$ and their enthalpy of formation from gaseous alkenes are small and positive (21 – 46 kJ mol^{-1} for C₂–C₄ alkene reactants, Table 2). These values reflect the difference between the energy required to rearrange the chemical bonds in the two ethene molecules in the TS and the energy recovered upon placing the TS structure in the vicinity of (Ni-OH)⁺ centers. Such stabilization is conferred by the combined effects of van der Waals (vdW) interactions and coordination at the acid-base site pair in active centers, which also affect the bound alkene monomers and are therefore reflected in their binding constants (β' , Eq. (15)). The vdW interactions become stronger for both the TS and the bound monomers with increasing size, while acid-base interactions are expected to be more localized and sense molecular

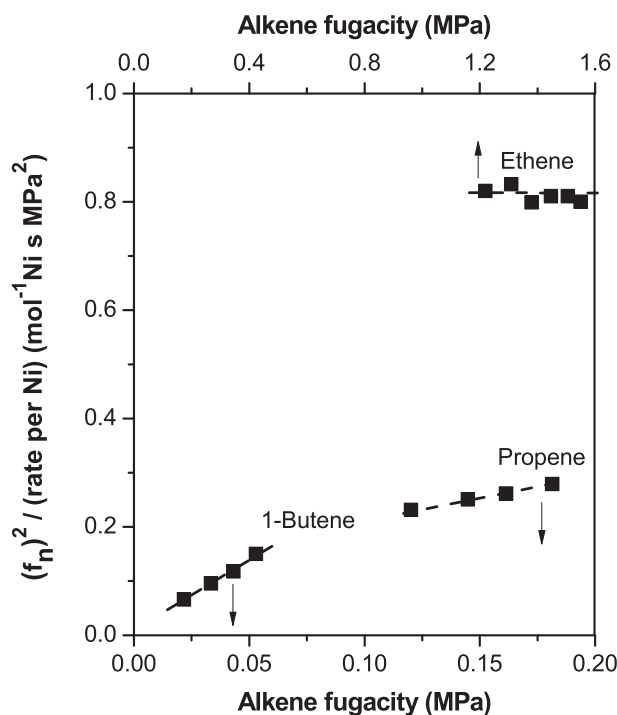


Fig. 7. The ratio of the square of alkene fugacity (f_n) to the dimerization rate (per active (Ni-OH)⁺ site) at 248 K as a function of alkene fugacity for ethene (top abscissa), propene and 1-butene (bottom abscissa) on small-pore Ni-Al-MCM-41 (pore diameter $1.7 \pm 0.5 \text{ nm}$, Ni²⁺:H₀⁺ = 5.0) in the presence of intrapore liquids ($P_i/P_{i,\text{sat}} = 0.7$ – 0.9). Dashed lines are the regression of the data to the functional form of Equation (13).

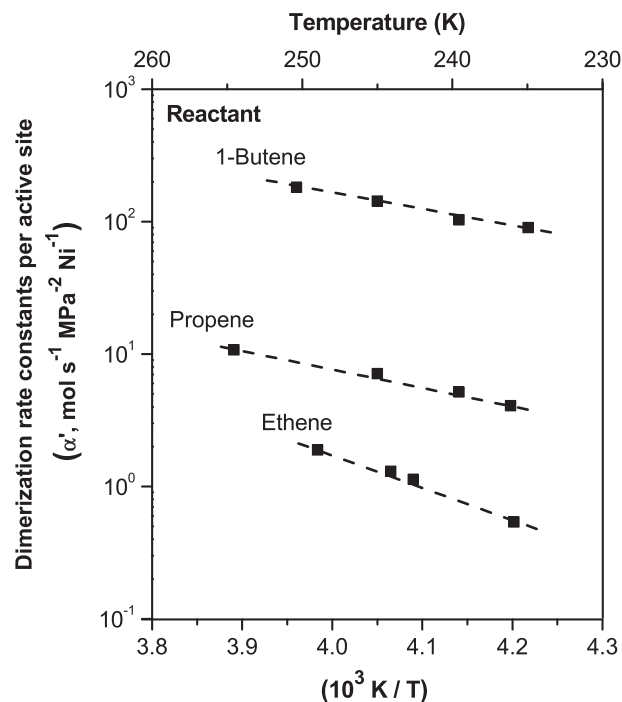


Fig. 8. Second-order alkene dimerization constants (per (Ni-OH)⁺ site) as a function of reciprocal temperature (bottom abscissa) and temperature (top abscissa) on small-pore Ni-Al-MCM-41 (1.7 nm mean diameter, Ni²⁺:H₀⁺ = 5.0) in the presence of intrapore liquids ($P_i/P_{i,\text{sat}} = 0.7$ – 0.9). Dashed lines correspond to the regression of the data to the form of Eq. (11).

size only through the weaker effects of chain length on the electron density at the alkene terminal π -bonds.

The weak binding of alkenes at $(\text{Ni-OH})^+$ centers is consistent with physisorption mediated by interactions of the vdW-type and with the enthalpy of adsorption (ΔH_{ads}) similar to those for their gas to liquid phase transition. Such physisorption processes occur with ΔH_{ads} values that are related to the enthalpy of condensation (ΔH_{cond}) by the parameter C in the Brunauer, Emmett and Teller (BET) adsorption isotherm (Eq. S7 and Fig. S6, SI, [54]):

$$C = \exp\left(\frac{\Delta H_{\text{ads}} - \Delta H_{\text{cond}}}{RT}\right) \quad (16)$$

The C value for each alkene was estimated from N_2 uptakes at 77 K on Ni-Al-MCM-41 and used here as a proxy for alkenes because of the non-specific nature of induced dipole forces and their similar role in determining interactions of molecules with surfaces and with like molecules in their liquid form. The C parameter for small-pore Ni-Al-MCM-41 was calculated from N_2 uptake data (Fig. 2) and combined with reported ΔH_{cond} values [55] to obtain estimates of ΔH_{ads} (Eq. (16)) for each alkene.

In using these ΔH_{ads} estimates to infer how measured ΔH^\ddagger values would vary with alkene size, we consider two asymptotic limits of a reactant-like early TS (one alkene in the liquid phase and one bound alkene) and a product-like late TS (one bound alkene dimer) by using their respective ΔH_{cond} values from their gaseous precursors. Fig. 9 shows measured ΔH^\ddagger as a function of the ΔH_{ads} values for each alkene for early and late C–C bond formation TS structures. As expected, ΔH_{ads} values become more negative with increasing alkene size, consistent with measured and DFT-derived binding constants and enthalpies of alkanes on large-pore zeolites [56], where alkane adsorbates are stabilized predominantly via vdW interactions with essentially flat surfaces; these effects of alkene size on ΔH_{ads} are also consistent with those

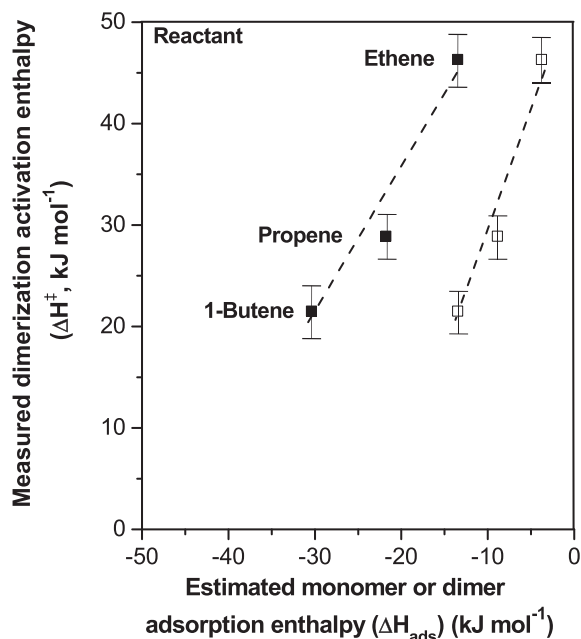


Fig. 9. Measured alkene dimerization activation enthalpies (ΔH^\ddagger) on small-pore Ni-Al-MCM-41 (1.7 nm mean diameter, $\text{Ni}^{2+}:\text{H}_0^+ = 5.0$) in the presence of intrapore liquids ($P_i/P_{i,\text{sat}} = 0.7\text{--}0.9$) for ethene, propene and 1-butene reactants at 248 K as a function of enthalpy of adsorption (ΔH_{ads}) of alkene reactants (\square) and of primary dimer products (1-butene for ethene, 1-hexene for propene, 1-octene for 1-butene, \blacksquare). ΔH^\ddagger determined from the regression of dimerization constants (Fig. 8) to the functional form of Equation (11). ΔH_{ads} derived from Equation (16) using C constant (obtained from Fig. S6, SI) and enthalpy of alkene condensation [55]. Dashed lines are used as trendline.

observed on measured alkene adsorption constants (β' , Table 2). Measured ΔH^\ddagger values decrease as ΔH_{ads} values becomes more negative (Fig. 9), as expected from interactions that become stronger with alkene size. The linear trends in Fig. 9, however, show slopes larger than unity, indicating that interactions other than vdW forces also stabilize TS structures via interactions with $(\text{Ni-OH})^+$ species and that they also become stronger with increasing molecular size. Along with vdW forces, these more specific interactions account for the effects of alkene size on measured dimerization rate constants (α' , Table 2).

The proton affinity (PA) of alkene monomers and dimers also increases with size, as known in catalysis by Brønsted acids involving proton transfer and carbenium ion TS structures [57]. We consider such properties (shown by α' values as a function of alkene PA (Fig. S12, SI)) not to be appropriate descriptors of alkene reactivity because $(\text{Ni-OH})^+$ species are expected to be much weaker Brønsted acids than aluminosilicates and there is no precedent for Brønsted acid-catalyzed dimerization catalysis at sub-ambient temperatures on such stronger acids [58].

The mechanistic conclusions related to alkene size effects can also be examined in the context of measured entropies of formation (ΔS^\ddagger , Table 2) of the C–C coupling TS, which reflect the entropy differences between the TS (S^\ddagger) and its two gaseous alkene precursors ($2S_n$) and their comparison to adsorption entropies calculated ($\Delta S_{\text{calc}}^\ddagger$) for weakly-bound hydrocarbons on oxides [59–61]; such physisorbed species retain about 70% of their gaseous translational and rotational entropies [62]. These estimates are calculated here for reactant-like early TS (ΔS_n^\ddagger) using the entropies of one bound monomer of one alkene in the liquid-phase and with respect to two gaseous alkenes, and for dimer-like late TS (ΔS_{2n}^\ddagger) using the entropies of bound primary alkene dimer products with respect to the entropies of two gaseous alkenes. Table 3 shows measured (ΔS^\ddagger) and calculated ($\Delta S_{\text{calc}}^\ddagger$) values for alkene reactants; both measured and calculated ΔS values decrease with alkene size, as expected from the enhanced loss of translational modes as large alkenes interact with active $(\text{Ni-OH})^+$ sites. Measured ΔS^\ddagger values are closer to those calculated for dimer-like TS structures (Table 3); these results are consistent with the premise that intrapore liquids do not affect the formation of a late, kinetically-relevant, dimer-like TS. These results also support the previous assumption that the activity coefficient for C–C bond formation TS (γ_i^\ddagger) is not very sensitive to the presence or absence of an intrapore liquid phase.

3.7. Effects of intrapore liquids on chain growth and oligomerization: Selectivity to primary and secondary products in reactions of ethene, propene, and 1-butene.

Fig. 10 shows the trimer (C_{3n}) to dimer (C_{2n}) molar ratios in the products formed from ethene, propene, and 1-butene reactants on small-pore Ni-Al-MCM-41 at different alkene fractional conver-

Table 3

Measured entropy changes upon formation of alkene dimerization TS structures from two gaseous alkene molecules (ΔS^\ddagger) on small-pore Ni-Al-MCM-41 ($\text{Ni}^{2+}:\text{H}_0^+ = 5.0$) at 237–257 K, and calculated entropy loss for reactant-like TS (ΔS_n^\ddagger) and product-like TS (ΔS_{2n}^\ddagger) from two gaseous alkenes.

Alkene reactant	Measured ΔS^\ddagger (J (mol K) ⁻¹) ^a	ΔS_n^\ddagger (J (mol K) ⁻¹) ^b	ΔS_{2n}^\ddagger (J (mol K) ⁻¹) ^b
Ethene	-103	-63	-126
Propene	-145	-76	-153
1-Butene	-187	-83	-166

^a ΔS^\ddagger derived from the regression of second order dimerization constants (Fig. 8) to the functional form of Eq. (11).

^b $\Delta S_{\text{calc}}^\ddagger$ values calculated for possible TS structures using entropies of translation and rotation for gas-phase alkenes and of condensation at 248 K [62–61].

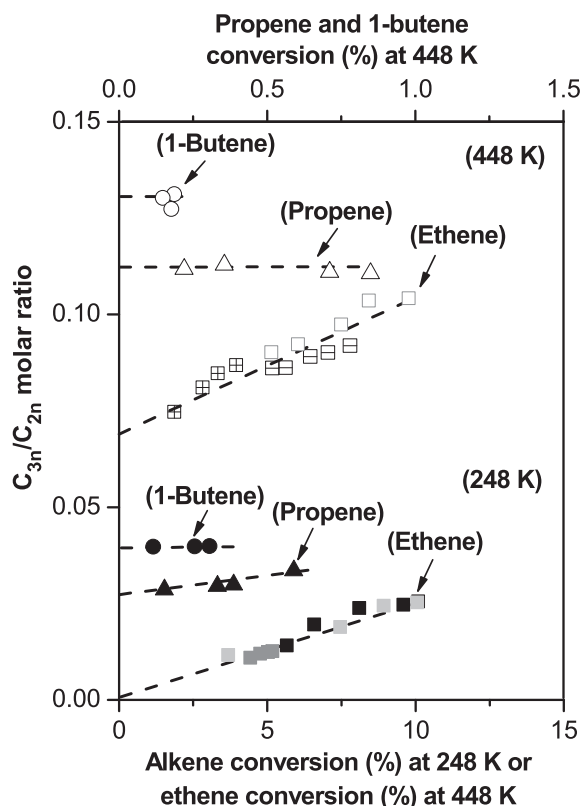


Fig. 10. Molar ratios of trimer (C_{3n}) and dimer (C_{2n}) products as a function of alkene conversion (%), varied through changes in bed residence time) on small-pore Ni-Al-MCM-41 at 248 K and 448 K. Filled symbols represent pores smaller than 2 nm filled with liquids (alkene $P_i/P_{i,sat} = 0.7\text{--}0.9$) and empty symbols denote conditions where pores contain gaseous reactants (as inferred from pore filling models, Fig. 2). C_{3n}/C_{2n} ratios for ethene shown for different Ni contents ($Ni^{2+}:H_0^+ = 0.1\text{--}5.0$), depicted by different square symbols, lighter to darker. C_{3n}/C_{2n} ratios for propene and 1-butene obtained for samples containing $Ni^{2+}:H_0^+ = 5.0$. C_{3n}/C_{2n} data for all alkenes at 448 K obtained under relatively stable rate conditions after an initial fast deactivation period. Dashed lines represent the regression the data to the linear trend predicted by Eq. (20).

sions (X_n), varied through changes in bed residence time (τ), at reaction conditions leading to the presence (248 K) or absence (448 K) of intrapore liquid alkenes. These C_{3n}/C_{2n} ratios extrapolated to zero conversion ($X_n \rightarrow 0$) increase from nearly zero for ethene to 0.03–0.04 for propene and 1-butene reactants at 248 K (Table 4, χ' defined in Eq. (21)), respectively, at conditions that cause the nearly complete filling of the MCM-41 mesopores with alkene reactants. These ratios reflect the likelihood that bound dimers undergo a subsequent C–C bond formation after their formation in the initial C–C coupling event, but before they desorb as the dimer product. These product ratios are significantly larger for each alkene at 448 K, than at 248 K (Table 4), an unexpected result

Table 4

χ' values, reflecting C_{3n} to C_{2n} ratios as $X_n \rightarrow 0$ (defined in Eq. (21)), obtained from the data in Fig. 10 during alkene dimerization reactions within small-pore Ni-Al-MCM-41 catalysts at 248 K (intrapore liquids) and at 448 K (gaseous conditions). The values in parentheses after each data refer to standard deviations from the data regression analyses to the functional form of Eq. (20).

Temperature (K)	Alkene reactant		
	Ethene	Propene	1-Butene
248 K	~0	0.030 (± 0.008)	0.040 (± 0.006)
448 K	0.070 (± 0.020)	0.110 (± 0.013)	0.130 (± 0.025)

because endothermic desorption events become favored as temperature increases over C–C bond formation events that exhibit a low activation barrier (ΔH^\ddagger , 21–46 kJmol⁻¹, Table 2), thus creating the expectation of a more probable desorption event before further growth at higher temperatures.

The C_{3n}/C_{2n} ratios for ethene (at both temperatures) and for propene (at 248 K) increase with increasing alkene conversions (Fig. 10), a reflection of the readsorption of their respective dimers and their subsequent growth along the catalyst bed. Such ratios for ethene reactants are the same at all Ni contents (0.1–5.0 $Ni^{2+}:H_0^+$, Fig. 10), indicative of the involvement of the same grafted (Ni-OH)⁺ sites in primary and secondary C–C coupling events. These C_{3n}/C_{2n} ratios are nearly invariant with conversion for propene at 448 K and for 1-butene at both temperatures, suggesting that the stronger binding of larger alkenes causes their slower (and nearly irreversible) desorption, which thus disfavors subsequent readsorption events along the catalyst bed.

Scheme 2 shows a reaction network that includes primary and secondary events during reactions of alkenes, along with the equilibrium and rate constants for all steps involved. Scheme 2 depicts:

- (i) the equilibrated adsorption (K_A) of alkene monomers (C_n) onto vacant (Ni-OH)⁺ sites ([Ni]) to give bound monomers (C_n^*)
- (ii) the formation of bound dimers (C_{2n}^* ; k_1) or bound isomeric species of the primary dimer isomer(s) ($i\text{-}C_{2n}^*$; k'_1) formed from C_n^* and an additional alkene monomer (C_n)
- (iii) the desorption (k_{D1}) of C_{2n}^* to give unbound dimers (C_{2n}) and vacant (Ni-OH)⁺ sites
- (iv) chain growth of C_{2n}^* with C_n into bound trimers (C_{3n}^*) via primary (k'_1) or secondary (k_2) reactions
- (v) desorption (k'_{D1}) of C_{3n}^* to give unbound trimers (C_{3n}) and vacant (Ni-OH)⁺ sites.

The effects of alkene conversion on C_{3n}/C_{2n} ratios (Fig. 10) are considered next in the context of the primary and secondary steps depicted in Scheme 2 using a mathematical framework appropriate for plug-flow reactors under conditions of relatively low conversions ($X_n < 0.1$). At such low reactant conversions, the concentration of the alkene reactants changes only slightly along the catalyst bed and the conversion (X_n) and bed residence time (τ , h·g_{cat}⁻¹·mol_{Cn}⁻¹) are related by (derived in Eqs. S47–S52, SI):

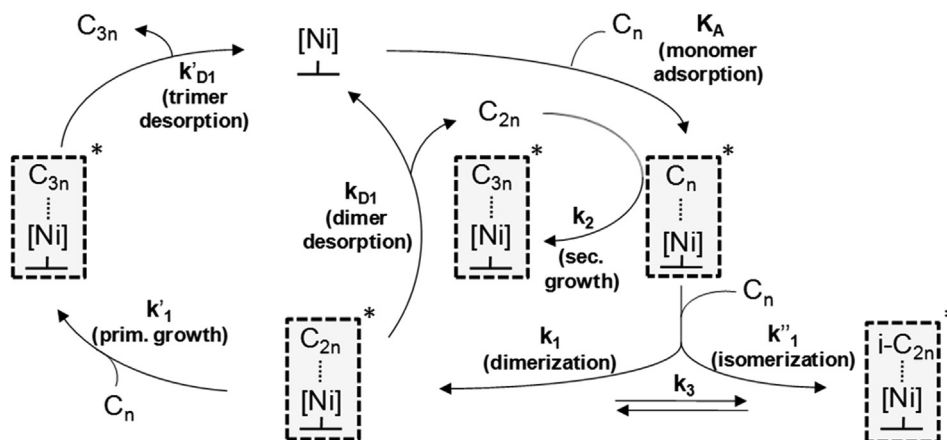
$$X_n = \alpha' f_{n0} \tau \quad (17)$$

where α' (Eq. (14)) is second-order dimerization rate constant (Table 2) and f_{n0} is alkene reactant fugacity at the reactor inlet (and the combined terms in the right side of Equation 17 are typically denoted as the Damköhler number). The reactions in Scheme 2 then lead to an expression for the dimer selectivity ($S_{C_{2n}}$, Eq. (2)) in a plug-flow reactor (for $X_n < 0.1$; derivation in Eqs. S20–S46, SI):

$$S_{C_{2n}} = \left[\frac{1}{\left(1 + \frac{3}{2} \frac{k'_1}{k_{D1}} f_{n0}\right)} \right] - \frac{1}{\alpha' f_{n0}} \left(\frac{k_2}{2k_1 + 3k'_1} \right) \cdot \left(\frac{f_{n0}}{1 + K_A f_{n0}} \right) X_n = S_0 - S_1 X_n \quad (18)$$

The molar ratio of trimer to dimer products (C_{3n}/C_{2n} , Fig. 10) reflects the combined effects of single-sojourn and multiple-sojourn events that form subsequent C–C bonds after the initial formation of dimers (as depicted in Scheme 2); this ratio can be represented as a function of alkene conversion (X_n) using the S_0 and S_1 terms:

$$\frac{C_{3n}}{C_{2n}} = \frac{1 - (S_0 - S_1 X_n)}{(S_0 - S_1 X_n)} \quad (19)$$



Scheme 2. Catalytic cycle for dimerization (C_{2n}), isomerization ($i-C_{2n}$) or chain-growth (C_{3n}) reactions of alkene reactants (C_n) onto $(Ni-OH)^+$ species ($[Ni]$).

The linear C_{3n}/C_{2n} trends in Fig. 10 reflect the small changes in this ratio with X_n and Eq. (19) can be rearranged into its asymptotic form (derivations in Eqs. S20–S52):

$$\frac{C_{3n}}{C_{2n}} = \chi' + X_n \frac{\frac{1}{\alpha'} (1 + \chi'^2) \left(\frac{k_2}{2k_1 + 3k_1} \right)}{(1 + K_A f_{n0})} = \chi' + S'_1 X_n \quad (20)$$

The χ' term reflects the intercept at $X_n \rightarrow 0$ in Fig. 10 and is defined by the following expression:

$$\chi' = \frac{3}{2} \frac{\left(\frac{K_1^* K_C}{\gamma_1^{\ddagger}} \right) f_{n0}}{\left(\frac{k_{D1}^{\ddagger}}{\gamma_{D1}^{\ddagger}} \right)} \quad (21)$$

where K_1^{\ddagger} is the rate constant for the formation of dimer chain growth TS, γ_1^{\ddagger} is the activity coefficient for dimer chain-growth TS, K_C is alkene condensation constant (only to be considered for intrapore liquids at 248 K), k_{D1}^{\ddagger} is desorption constant for dimer desorption TS, γ_{D1}^{\ddagger} is the activity coefficient for dimer desorption TS.

The small χ' (Eq. (21)) values at 248 K (<0.04 , Table 4) show that bound dimers desorb in most instances before any subsequent chain growth at these temperatures when intrapore liquids are present because of the effects of such liquids on dimer desorption TS structures and their preferential effects on γ_{D1}^{\ddagger} relative to the activity coefficient for the C–C formation TS (γ_1^{\ddagger}), as evident from the form of Eq. (21). The preferential enhancement of dimer desorption over its subsequent C–C bond formation reflects the late nature of the desorption TS and its product-like character, which places the TS, at least in part, within the liquid phase that ultimately solvates the desorbed primary dimer product. The TS that mediates the reaction of the bound dimer with another alkene, however, occurs earlier along the reaction coordinate and mediates the interconversion of bound species; its activity coefficient (γ_1^{\ddagger} , Eq. (21)) is much less sensitive, as a result, to the presence of a liquid phase than for the late dimer desorption TS. The higher χ' values measured at 448 K (0.07–0.13, Table 4) reflect a greater probability of subsequent dimer growth before desorption, in spite of expectations that higher temperatures would favor desorption over C–C formation steps with very low barriers (Table 2), a likely indication that the absence of a liquid phase leads to much less stable desorption TS than when liquids are present and preferentially stabilize such late transition states. At a given temperature, the effects of alkene size on χ' (Table 4) reflect the stronger binding and less favorable desorption of the larger alkene dimers formed from propene and 1-butene reactants, which renders desorption slower and less reversible than for the butene molecules formed from ethene reactants. Such binding

effects show direct consequences on catalyst stability when evaluated under gaseous conditions at 248 K, leading to deactivation constants (k_d) that markedly increase with size (at $P_i/P_{i,sat}$ below 0.60–0.65, Fig. 3).

The observed increase in C_{3n}/C_{2n} ratios with increasing alkene conversion (X_n , Fig. 10) reflects the readsorption of dimers (C_{2n}) along the catalyst bed, thus enabling additional opportunities for chain growth (Scheme 2). Readsorption is mediated by the same TS as the desorption steps that detach dimers from $(Ni-OH)^+$ binding sites. The C_{3n}/C_{2n} values for propene and 1-butene reactants are nearly independent of their respective conversion (Fig. 10), a result of a small S'_1 value in Equation (20). The magnitude of S'_1 decreases with increasing alkene size because α' values increase with size (Table 2) and dimer desorption becomes less reversible for larger alkenes, leading to a lower probability of readsorption along the bed and subsequent growth (k_2 , Scheme 2). In addition, the $(1 + K_A f_{n0})$ term in S'_1 (Eq. (20)) increases with alkene size because of the stronger binding of larger alkenes (~ 1 , ethene; 1.9, propene; 22.0, 1-butene), even though reactions of the larger alkenes were carried out at much lower pressures, thus leading to the smaller slopes of C_{3n}/C_{2n} ratios with conversion for larger alkenes. The effects of temperature on the slopes of C_{3n}/C_{2n} trends with conversion (Fig. 10) are very small, apparently as a result of a fortuitous cancellation of the effects of temperature on the various terms in Eq. (20).

The skeletal isomers and regioisomers of the dimers first formed in C–C coupling events can rearrange before desorption or via subsequent sojourns mediated by readsorption. Such dimer readsorption events dictate the extent to which isomer distributions will vary with changes in reactant conversion and bed residence time. Previous studies of ethene reactions showed that 1-butene is the sole primary product at 248 K and that 2-butene isomers form only via secondary isomerization reactions mediated by 1-butene readsorption [28].

Fig. 11 shows the ratios of C_6 isomer products to *trans*-2-hexene (for ethene, Fig. 11a) and *trans*-4-methyl-2-pentene (for propene, Fig. 11b), the most prevalent isomers formed in each case as a function of ethene (as a secondary product of ethene-butene molecules) or propene (as the propene dimer formed) reactant conversions at 248 K in the presence of ethene or propene as intrapore liquids on small-pore Ni-Al-MCM-41 catalysts with 0.2 and 5.0 $Ni^{2+}:H_0^+$ ratios. C_6 isomer ratios are similar for both $Ni^{2+}:H_0^+$ for both alkene reactants, indicating the exclusive involvement of $(Ni-OH)^+$ sites in C_6 isomerization reactions at 248 K. Linear hexenes are predominant C_6 isomers formed in ethene reactions from the reactions of 1-butene (the primary dimer) [28] with ethene in secondary reactions mediated by 1-butene readsorption along

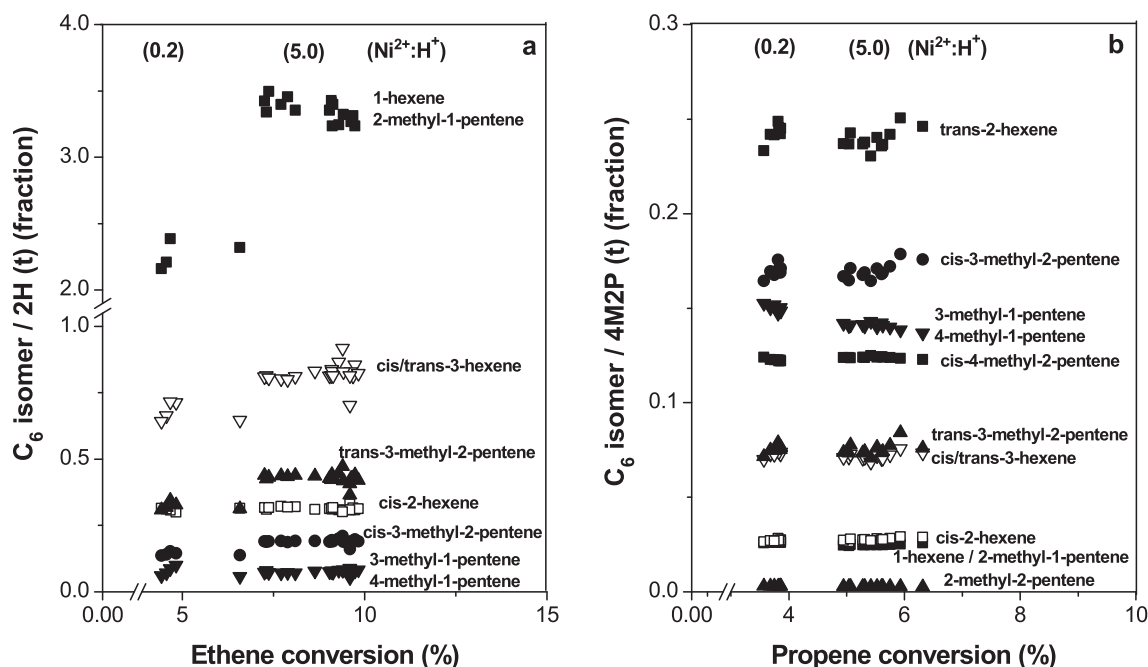


Fig. 11. Molar ratio of C_6 isomers for ethene (Fig. 11a) and propene (Fig. 11b) reactants as a function of reactant conversion at 248 K on small-pore Ni-Al-MCM-41 samples containing $Ni^{2+}:H_0^+$ ratios of 0.2 and 5.0. C_6 isomer ratios measured during ethene and propene dimerization in the presence of intrapore liquids ($P_i/P_{i,sat} = 0.7-0.9$). C_6 isomers shown for 2-methyl-2-pentene (2M2P), *trans*-4-methyl-2-pentene (4M2P (t)), *cis*-4-methyl-2-pentene (4M2P (c)), *cis*-3-methyl-2-pentene (3M2P (c)), *trans*-3-methyl-2-pentene (3M2P (t)), 1-hexene (1H), 2-methyl-1-pentene (2M1P), *cis*-2-hexene (2H (c)), *trans*-2-hexene (2H (t)), *cis/trans*-3-hexene (3H (c/t)), 3-methyl-1-pentene (3M1P), 4-methyl-1-pentene (4M1P). 3M1P/4M1P and 1H/2M1P are shown as lumped because they cannot be distinguished via gas-chromatography.

the catalyst bed. C_6 isomer ratios increase with conversion before stabilizing at *ca.* 7% conversion. The initial increase reflects the monotonic increase in C_6 alkene concentration with conversion, which enables their readsorption and isomerization; at higher conversions, the products reach their equilibrium distributions and become independent of conversion, leading to isomerization approach to equilibrium values (η_{C_6}) near unity for most linear isomers (248 K; Table 5, thermodynamic data obtained from [63]). Such η_{C_6} values reflect fast C_6 isomerization reactions on

(Ni-OH)⁺ sites, unlike linear C_4 isomerization reactions that occur less likely because of their more facile desorption than bound C_6 isomers, leading to lower approach to equilibrium values for C_4 isomerization ($\eta_{C_4} \sim 0.1$) during ethene dimerization at 248 K [28].

trans-4-methyl-2-Pentene is the most abundant hexene isomer formed from propene reactants and the ratios of all other isomers to this predominant isomer are insensitive to propene conversion on Ni-Al-MCM-41 and similar for samples with 0.2 and 5.0 $Ni^{2+}:H_0^+$ at 248 K (Fig. 11b). Only linear and monomethyl hexenes are

Table 5

Measured molar ratios of C_6 isomers for ethene and propene reactants at 6% conversion on small-pore Ni-Al-MCM-41 ($Ni^{2+}:H_0^+ = 5.0$) in the presence of intrapore liquids at 248 K and the corresponding equilibrium ratios obtained from [63]. 2H (t) *trans*-2-hexene and 4M2P (t) is *trans*-4-methyl-2-pentene. 1-hexene and 2-methyl-1-pentene are shown together because the chromatographic column used in this study (described in Section 2.3) does not allow their separation.

C_6 isomer	Measured for ethane C_6 isomer/2H (t)	Equilibrium C_6 isomer/2H (t)	Measured for propene C_6 isomer/4M2P (t)	Equilibrium C_6 isomer/4M2P (t)
Linear isomers				
1-hexene	3.38	5.1	0.02	0.57
2-methyl-1-pentene				
<i>cis</i> -2-hexene	0.31	0.27	0.03	0.03
<i>trans</i> -2-hexene	reference	reference	0.25	0.23
<i>cis</i> -3-hexene	0.89	0.50	0.08	0.09
<i>trans</i> -3-hexene				
Monomethyl isomers				
3-methyl-1-pentene	0.07	0.04	0.14	0.10
4-methyl-1-pentene				
2-methyl-2-pentene	n.d. ^a	83.00	0.01	18.30
<i>cis</i> -3-methyl-2-pentene	0.19	24.0	0.18	5.80
<i>trans</i> -3-methyl-2-pentene	0.43	46.00	0.08	10.20
<i>cis</i> -4-methyl-2-pentene	n.d. ^a	1.30	0.12	0.16
<i>trans</i> -4-methyl-2-pentene	n.d. ^a	4.50	reference	reference
Ethyl and dimethyl isomers				
2-ethyl-1-butene	n.d. ^a			
2,3-Dimethyl-1-butene	n.d. ^a	n.d. ^a	n.d. ^a	n.d. ^a
3,3-Dimethyl-1-butene	n.d. ^a	n.d. ^a	n.d. ^a	n.d. ^a
2,3-Dimethyl-2-butene	n.d. ^a	n.d. ^a	n.d. ^a	n.d. ^a

^a Isomer not detected.

detected as propene dimerization products (Table 5). These isomers are not formed at the ratios predicted from the thermodynamics of their gaseous forms. The invariance of C₆ isomers with conversion indicates that they can form via rearrangements of dimer TS structures or of bound dimers before desorption and that their desorption is essentially irreversible; these dimers do not significantly readsorb and isomerize along the catalyst bed, indicative of isomerization steps that are much faster than subsequent C–C coupling events. These data cannot inform about whether these isomers form directly at C–C coupling TS structures or via fast rearrangements before dimer desorption, but their relative concentrations do not reflect the thermodynamics of the interconversion among these isomers (Table 5); they reflect instead their relative abundance as bound species weighed by the desorption rate constants of each bound isomer. We surmise that the acid-base character of (Ni-OH)⁺ sites, leading to concerted effects from O- and H-atoms, can lead to such C₆ products in the first alkene surface sojourn.

The C₆ isomers differ when they are formed from butene-ethene and propene-propene C–C coupling reactions (Table 5). These differences seem to reflect the extent to which interactions of these two pairs with acid-base moieties at (Ni-OH)⁺ sites change the electron density at the various C-atoms in the two molecules involved, in order to create nucleophilic (electron rich) and electrophilic (electron-deficient) C-atoms that determine the positions at the new C–C bond forms. These trends, as well as the unique reactivity of (Ni-OH)⁺ species in C–C coupling reactions, are being explored through theoretical treatments that we expect will be the subject of a later report.

4. Conclusions

This work reports mechanistic insights on the consequences of intrapore alkene liquids on the reactivity and stability of active Ni species during C₂–C₄ alkene dimerization reactions on Ni-Al-MCM-41 catalysts at subambient temperatures. This work extends previous findings for intrapore ethene liquids, which stabilize active Ni species via the preferential solvation of late transition states (TS) that mediate dimer desorption steps, to larger alkene reactants (C₃–C₄), which also form intrapore liquids that confer stability via analogous solvation effects even though these larger alkenes react faster and produce oligomers that bind stronger than ethene reactants. Such intrapore alkene liquids lead to unprecedented catalyst mean lives (>600 h) at 248 K in comparison to reported Ni-based metal-organic frameworks or aluminosilicates operating at higher temperatures.

Stable dimerization rates are obtained on Ni-Al-MCM-41 catalysts containing small or large mesopores when alkene pressures are adjusted to those required for capillary condensation, as determined by alkene pore filling models. Such stabilization effects are facilitated by weak van der Waals interactions between dimer desorption TS and the surrounding intrapore liquid phase, irrespective of whether such liquids consist of pure alkenes or of unreactive alkanes mixed with their alkene reactant counterparts, suggesting the non-specificity of the interactions responsible for such solvation.

Such stability allows accurate inquiries into the elucidation of the active Ni species responsible for dimerization catalysis. Such inquiries are achieved by systematic variations of Ni loading via Ni²⁺ cation exchange within isolated H⁺ positions in parent Al-MCM-41 aluminosilicates and via Ni atom deposition after all initial H⁺ sites are titrated. Dimerization rates (per Ni) do not vary with Ni content until all H⁺ sites are exchanged by (Ni-OH)⁺ sites, identified as the most plausible active species given the isolated nature of the H⁺ precursors. A marked per Ni rate decrease is

observed for Ni loadings above exchange stoichiometry, indicative of the presence of NiO moieties without any catalytic activity.

Stable rates also allow accurate mechanistic assessments of the elementary steps that mediate dimerization reactions in the presence of intrapore liquids. Transition state theory formalisms appropriate for thermodynamically non-ideal conditions together with the effects of alkene size on second-order dimerization rate constants and alkene monomer adsorption constants enable the identification of the kinetically relevant TS as occurring late along reaction coordinates and resembling the dimer products in the surrounding liquid.

The presence of intrapore non-ideal liquids shows marked consequences on the solvation of bound dimer desorption TS structures. Such solvation effects are predominantly evident during the first alkene surface sojourn, resulting in much higher dimer selectivities at 248 K (>90%) than at higher temperatures, and demonstrate the relevance of dimer adsorption-desorption steps on selectivity. Dimer selectivities decrease as the concentration of unbound dimer products increases, a consequence of secondary dimer readsorption and chain-growth events. The distributions of C₆ isomers from ethene and propene reactants, formed in secondary and primary reaction events, respectively, provide additional evidence for the irreversibility of dimer desorption steps. Propene dimers rearrange into equilibrated mixtures of C₆ isomers even before desorbing from the catalyst surface mediated by acid-base interactions from the O–H moiety within active (Ni-OH)⁺ species.

Declaration of Competing Interest

The authors declare that they have no known competing financial interests or personal relationships that could have appeared to influence the work reported in this paper.

Acknowledgements

The authors acknowledge a Marie Skłodowska Curie Individual Fellowship (COUPCAT project, H2020 Program) and the Vermeulen Chair endowment fund for the financial support used to carry out the research. We are also grateful to Drs. Michele Sarazen, Gina Noh and Shuai Wang for technical discussions.

Appendix A. Supplementary data

Supplementary data to this article can be found online at <https://doi.org/10.1016/j.jcat.2020.06.038>.

References

- [1] J. Skupinska, *Chem. Rev.* 91 (1991) 613–648.
- [2] D.S. McGuinness, *Chem. Rev.* 111 (2011) 2321–2341.
- [3] D.J. Parrillo, C. Lee, R.J. Gorte, D. White, W.E. Farneth, *J. Phys. Chem.* 99 (1995) 8745–8749.
- [4] S. Svelle, S. Kolboe, O. Swang, *J. Phys. Chem. B* 108 (2004) 2953–2962.
- [5] P. Oliveira, P. Borges, R.R. Pinto, M. Lemos, F. Lemos, J.C. Vedrine, F.R. Ribeiro, *Appl. Catal. A– General* 384 (2010) 177–185.
- [6] M.L. Sarazen, E. Doskocil, E. Iglesia, *J. Catal.* 344 (2016) 553–569.
- [7] M.L. Sarazen, E. Iglesia, *ACS Catal.* 6 (2016) 7059–7070.
- [8] K. Ziegler, E. Holzkamp, H. Breil, H. Martin, *Angew. Chem. Int. Ed.* 67 (1955) 541–547.
- [9] Z.B. Guan, P.M. Cotts, E.F. McCord, S.J. McLain, *Science* 283 (5410) (1999) 2059–2062.
- [10] D.L. Beach, Y.V. Kissin, US4686315A.
- [11] H.K.C. Timken, B.K. Chang, C.B. Campbell, A.M. Thomas, M.A. Fernandez, M. Sessions, WO2016160839A1.
- [12] R. Robinson Jr., D.S. McGuinness, B.F. Yates, *ACS Catal.* 3 (2013) 3006–3015.
- [13] F. Speiser, P. Braunstein, L. Saussine, *Acc. Chem. Res.* 38 (2005) 784–793.
- [14] M. Klapper, D. Joe, S. Nietzel, J.W. Krumpfer, K. Müller, *Chem. Mater.* 26 (2014) 802.
- [15] T.F. McKenna, J.B.P. Soares, *Chem. Eng. Sci.* 56 (2001) 3931–3949.

- [16] C.M. Killian, L.K. Johnson, M. Brookhart, *Organometallics* 16 (1997) 2005–2007.
- [17] J.A. Suttill, D. McGuinness, *Organometallics* 31 (2012) 7004–7010.
- [18] A. Kermagoreta, R.N. Kerberb, M.P. Conleyc, E. Callensa, P. Floriand, D. Massiotd, F. Delbecqb, X. Rozanskab, C. Copéret, *J. Catal.* 313 (2014) 46–54.
- [19] S.T. Madrahimov, J.R. Gallagher, G. Zhang, Z. Meinhart, S.J. Garibay, M. Delferro, J.T. Miller, O.K. Farha, J.T. Hupp, S.T. Nguyen, *ACS Catal.* 5 (2015) 6713–6718.
- [20] J. Canivet, S. Aguado, Y. Schuurman, D. Farrusseng, *J. Am. Chem. Soc.* 135 (2013) 4195–4198.
- [21] E.D. Metzger, R.J. Comito, Z. Wu, G. Zhang, R.C. Dubey, W. Xu, J.T. Miller, M. Dinca, A.C.S. Sust, *Chem. Eng.* 7 (2019) 6654–6661.
- [22] R.D. Andrei, M.I. Popa, F. Fajula, V. Hulea, *J. Catal.* 323 (2015) 76–84.
- [23] M. Lallemand, A. Finiels, F. Fajula, V. Hulea, *Stud. Surf. Sci. Catal.* 170 (2007) 1863–1868.
- [24] M. Lallemand, A. Finiels, F. Fajula, V. Hulea, *Chem. Eng. J.* 172 (2011) 1078–1082.
- [25] S. Lin, L. Shi, H. Zhang, N. Zhang, X. Yi, A. Zheng, X. Li, *Micropor. Mesopor. Mater.* 184 (2014) 151–161.
- [26] A. Lacarriere, J. Robin, D. Swierczynski, A. Finiels, F. Fajula, F. Luck, V. Hulea, *ChemSusChem* 5 (2012) 1787–1792.
- [27] S. Moussa, M.A. Arribas, P. Concepción, A. Martínez, *Catal. Today* 277 (2016) 78–88.
- [28] I. Agirrezabal-Telleria, E. Iglesia, *J. Catal.* 352 (2017) 505–514.
- [29] M. Lallemand, O.A. Rusu, E. Dumitriu, A. Finiels, F. Fajula, V. Hulea, *Appl. Catal. A* 338 (2008) 37–43.
- [30] R. Joshi, G. Zhang, J.T. Miller, R. Gounder, *ACS Catal.* 8 (2018) 11407–11422.
- [31] A. Ehrmaier, Y. Liu, S. Peitz, A. Jentys, Y.-H.C. Chin, M. Sanchez-Sanchez, R. Bermejo-Deval, J. Lercher, *ACS Catal.* 9 (2019) 315–324.
- [32] R.Y. Brogaard, U. Olsbye, *ACS Catal.* 6 (2016) 1205–1214.
- [33] G. Mathys, J.S. Godsmark, M. Janssen, L.R. Martens, H.J. Beckers, E. T.A. Van Driessche, R.F. Ivo Caers, J.R. Shutt, US6770791B2.
- [34] D.A. Young, D.E. Vaughan, R.L. Pruet, M.E. Tunison, US5108970A.
- [35] D.L. Beach, T.P. Kobylinski, US4293726A.
- [36] A.A. Davydov, M. Kantcheva, M.L. Chepotko, *Catal. Lett.* 83 (2002) 97–108.
- [37] M. Lallemand, A. Finiels, F. Fajula, V. Hulea, *J. Phys. Chem. C* 113 (2009) 20360–20364.
- [38] V. Hulea, F. Fajula, *J. Catal.* 225 (2004) 213–222.
- [39] A. Finiels, F. Fajula, V. Hulea, *Catal. Sci. Technol.* 4 (2014) 2412–2426.
- [40] A.N. Mlinar, S. Shylesh, O.C. Ho, A.T. Bell, *ACS Catal.* 4 (2014) 337–343.
- [41] A.N. Mlinar, G.B. Baur, G.G. Bong, A.B. Getsoian, A.T. Bell, *J. Catal.* 296 (2012) 156–164.
- [42] J. Rabeah, J. Radnik, V. Briois, D. Maschmeyer, G. Stochniol, S. Peitz, H. Reeker, C. La Fontaine, A. Brückner, *ACS Catal.* 6 (2016) 8224–8228.
- [43] J.S. Beck, J.C. Vartuli, W.J. Roth, M.E. Leonowicz, C.T. Kresge, K.D. Schmitt, C.T.-W. Chu, D.H. Olson, E.W. Sheppard, S.B. McCullen, J.B. Higgins, J.L. Schlenke, *J. Am. Chem. Soc.* 114 (1992) 10834–10843.
- [44] C.D. Baertsch, K.T. Komala, Y.H. Chua, E. Iglesia, *J. Catal.* 205 (2002) 44–57.
- [45] L. Soják, G. Addová, R. Kubinec, A. Kraus, G. Hu, *J. Chromatogr. A* 947 (2002) 103–117.
- [46] M. Sarazen, E. Iglesia, *PNAS* 114 (2017) E3900–E3908.
- [47] The Vapor pressures of some hydrocarbons in the liquid and solid state at low temperatures, W.T. Ziegler (1959), U.S. National Bureau of Standards.
- [48] E.P. Barrett, L.G. Joyner, P.P. Halenda, *J. Am. Chem. Soc.* 73 (1951) 373–380.
- [49] R.J. Madon, E. Iglesia, *J. Mol. Catal. A Chem.* 163 (2000) 189–204.
- [50] J.B. Butt, *Reaction Kinetics and Reactor Design*, 2nd Edition, Marcel Dekker, 2000, pp. 113–150.
- [51] C.A. Eckert, M. Boudart, *Chem. Eng. Sci.* 18 (1963) 144.
- [52] E.F. Obert, *Thermodynamics*, McGraw Hill 1948 New York.
- [53] E.E. Gonzo, M. Boudart, *J. Catal.* 52 (1978) 462.
- [54] S. Brunauer, S. Emmett, P.H. Teller, *J. Am. Chem. Soc.* 60 (1938) 309–319.
- [55] J.S. Chickos, W.E. Acree Jr., *J. Phys. Chem. Ref. Data*, 32 (2003) No. 2.
- [56] B.A. De Moor, M.F. Reyniers, O.C. Gobin, J.A. Lercher, G.B. Marin, *J. Phys. Chem. C* 115 (2011) 1204–1219.
- [57] P. Deshlahra, E. Iglesia, *ACS Catal.* 6 (2016) 5386–5392.
- [58] M.L. Sarazen, E. Iglesia, *ChemCatChem* 10 (2018) 4028–4037.
- [59] E.P.L. Hunter, S.G. Lias, *J. Phys. Chem. Ref. Data*, 27(3) (1998)
- [60] R.A. Alberty, C.A. Gehrig, *J. Phys. Chem. Ref. Data*, 14(3) (1985).
- [61] J.E. Kilpatrick, K.S. Pitzer, *J. Res. Natl. Bur. Stand.* 37 (1946) 163–171.
- [62] C.T. Campbell, J.R.V. Sellers, *Chem. Rev.* 113 (2013) 4106–4135.
- [63] J.E. Kilpatrick, E.J. Prosen, K.S. Pitzer, F.D. Rossini, *J. Res. Natl. Bur. Stand.* 36 (1946) 584.